Primary Production, an Index of Climate Change in the Ocean: Satellite-Based Estimates over Two Decades

Gemma Kulk[1]*[iD], Trevor Platt[1], James Dingle[1], Thomas Jackson[1], Bror Jönsson[1], Heather A. Bouman[2], Marcel Babin[3], Robert J. W. Brewin[4], Martina Doblin[5], Marta Estrada[6], Francisco G. Figueiras[7], Ken Furuya[8], Natalia González-Benítez[9], Hafsteinn G. Gudfinnsson[10], Kristinn Gudmundsson[10], Bangqin Huang[11], Tomonori Isada[12], Žarko Kovač[13], Vivian A. Lutz[14], Emilio Marañón[15], Mini Raman[16], Katherine Richardson[17], Patrick D. Rozema[18], Willem H. van de Poll[18], Valeria Segura[14], Gavin H. Tilstone[1], Julia Uitz[19], Virginie van Dongen-Vogels[20], Takashi Yoshikawa[8] and Shubha Sathyendranath[21]

[1] Earth Observation Science and Applications, Plymouth Marine Laboratory, Prospect Place, The Hoe, Plymouth, PL1 3DH, UK; gku@pml.ac.uk (G.K.), tplatt@dal.ca (T.P.), jad@pml.ac.uk (J.D.), thja@pml.ac.uk (T.J.), brj@pml.ac.uk (B.J.), ghti@pml.ac.uk (G.H.T.)
[2] Department of Earth Sciences, University of Oxford, Oxford, OX1 3AN, UK; heather.bouman@earth.ox.ac.uk
[3] Marine Optics and Remote Sensing Lab, Laboratoire d'Océanographie de Villifranche, B.P. 8, Quai de la Darse, Villefranche-sur-Mer, CEDEX 06238, France; marcel@obs-vlfr.fr
[4] College of Life and Environmental Sciences, University of Exeter, Peter Lanyon Building, Treliever Road, Penryn, Cornwall, TR10 9FE, UK; R.Brewin@exeter.ac.uk
[5] Plant Functional Biology and Climate Change Cluster, Faculty of Science, University of Technology Sydney, P.O. Box 123 Broadway, Sydney, NSW 2007, Australia; Martina.Doblin@uts.edu.au
[6] Institut de Ciències der Mar, CSIC, Pg. Marítim de la Barceloneta, 37-49, 08003 Barcelona, Spain; marta@icm.csic.es
[7] Instituto de Investigaciones Marinas, CSIC, Eduardo Cabello 6, 36208 Vigo, Spain; paco@iim.csic.es
[8] Graduate School of Agricultural and Life Sciences, The University of Tokyo, Tokyo 113-8657, Japan; furuya@fs.a.u-tokyo.ac.jp (K.F.); undaria@scc.u-tokai.ac.jp (T.Y.)
[9] Area of Biodiversity and Conservation, Universidad Rey Juan Carlos, Tulipán, E-28933 Madrid, Spain; natalia.gonzalez@urjc.es
[10] Marine and Freshwater Research Institute, Skúlagata 4, 101 Reykjavík, Iceland; hafsteinn.gudfinnsson@hafogvatn.is (H.G.G.), kristinn.gudmundsson@hafogvatn.is (K.G.)
[11] State Key Laboratory of Marine Environmental Science, Fujian Provincial Key Laboratory of Coastal Ecology and Environmental Studies, Xiamen University, Xiamen, Fujian, 361005, China; bqhuang@xmu.edu.cn
[12] Akkeshi Marine Station, Field Science Center for Nothern Biosperhe, Hokkaido University, Aikkapu 1, Akkeshi, Hokkaido, Japan; t-isada@fsc.hokudai.ac.jp
[13] Faculty of Science, University of Split, Rudera Boškovića 33, 21000 Split, Croatia; zarko.kovac@pmfst.hr
[14] Instituto Nacional de Investigacion y Desarrollo Pesquero, Mar del Plata, Argentina; vlutz@inidep.edu.ar (V.A.L.), vsegura@inidep.edu.ar (V.S.)
[15] Departamento de Ecoloxía e Bioloxía Animal, Universidade de Vigo, Campus As Lagoas-Marcosende, 36310 Vigo (Pontevedra), Spain; em@uvigo.es
[16] Space Application Center, ISRO, Jodhpur Tekra, Ambawadi Vistar P.O., Ahmedabad – 380015, India; mraman@sac.isro.gov.in
[17] Center for Macroecology, Evolution and Climate, Globe Institute, University of Copenhagen, Universitetsparken 15, 2100 Copenhagen, Denmark; kari@science.ku.dk
[18] Department of Ocean Ecosystems, Energy and Sustainability Research Institute Groningen, University of Groningen, Nijenborgh 7, 9747 AG Groningen, The Netherlands; p.d.rozema@gmail.com (P.D.R.), w.h.van.de.poll@rug.nl (W.H.P.)
[19] CNRS and Sorbonne Université, Laboratoire d'Océanographie de Villefranche, LOV, 06230 Villefranche-sur-mer, France; julia.uitz@obs-vlfr.fr

20　Oceanography and Shelf Processes Research, Australian Institute of Marine Science, PMB3, Townsville MC
　　QLD 4810, Australia; v.vandongenvogels@aims.gov.au
21　National Centre for Earth Observation, Plymouth Marine Laboratory, Prospect Place, The Hoe, Plymouth,
　　PL1 3DH, UK; ssat@pml.ac.uk
*　Correspondence: gku@pml.ac.uk; Tel.: +44 (0)1752 633427

Abstract: Primary production by marine phytoplankton is one of the largest fluxes of carbon
on our planet. In the past decades, considerable progress has been made in estimating global
primary production at high spatial and temporal scales by combining *in situ* measurements of
primary production with remote-sensing observations of phytoplankton biomass. One of the major
challenges in this approach lies in the assignment of the appropriate model parameters that define the
photosynthetic response of phytoplankton to the light field. In the present study, a global database of
in situ measurements of photosynthesis versus irradiance (P-I) parameters and a 20-year record of
climate quality satellite observations were used to assess global primary production and its variability
with seasons and locations as well as between years. In addition, the sensitivity of the computed
primary production to potential changes in the photosynthetic response of phytoplankton cells under
changing environmental conditions was investigated. Global annual primary production varied
from 38.8 to 42.1 Gt C yr^{-1} over the period of 1998-2018. Inter-annual changes in global primary
production did not follow a linear trend and regional differences in the magnitude and direction of
change in primary production were observed. Trends in primary production followed directly from
changes in chlorophyll-*a* and were related to changes in the physico-chemical conditions of the water
column due to inter-annual and multi-decadal climate oscillations. Moreover, the sensitivity analysis
in which P-I parameters were adjusted by ± 1 standard deviation showed the importance of accurately
assigning photosynthetic parameters in global and regional calculations of primary production. The
assimilation number of the P-I curve showed strong relationships with environmental variables
such as temperature and had a practically one-to-one relationship with the magnitude of change
in primary production. In the future, such empirical relationships could potentially be used for a
more dynamic assignment of photosynthetic rates in the estimation of global primary production.
Relationships between the initial slope of the P-I curve and environmental co-variables were more
elusive.

Keywords: Primary Production; Phytoplankton; Photosynthesis; Ocean-colour Remote-sensing;
Climate Change

1. Introduction

The oceans play a key role in biogeochemical processes on Earth. Phytoplankton are responsible for
almost half of the total global net primary production [1–5]. This does not only provide the basis for
the marine food web, but also has a strong impact on carbon sequestration in the ocean's interior [6].
Marine primary production, estimated to be of the order of 50 Gt C per annum [2–5,7], is one of the
largest fluxes of carbon on our planet. Because of its importance, phytoplankton primary production
has received considerable attention from the scientific community. Studies based on *in situ* observations
are now supplemented by satellite-based calculations to estimate global primary production patterns
at high spatial and temporal resolutions. Yet, trends in biological fields estimated from remote-sensing
observations have not been taken into account in recent studies on global carbon budgets and pools
and fluxes of carbon in the ocean [8,9]. In recent years, considerable efforts have been made to correct
inter-sensor biases and merge data from multiple ocean-colour satellite sensors to provide a long (over
two decades) record of phytoplankton biomass in the global oceans through the Ocean Colour Climate

Change Initiative of the European Space Agency [10]. This time series now offers the opportunity to undertake a systematic study of changes in phytoplankton primary production over the last 20 years.

Phytoplankton primary production is forced by physico-chemical conditions in the water column, including temperature, light and micro- and macronutrients. These drivers are influenced by seasonal, inter-annual and multi-decadal variations in oceanic and atmospheric processes. For example, phytoplankton primary production in polar regions is strongly influenced by seasonal solar irradiance patterns and the formation of surface mixed layers due to ice melt in spring and summer [11–14]. In contrast, at lower latitudes where trade winds prevail, phytoplankton primary production can be nutrient-limited year-round and seasonal patterns are less obvious [15,16]. Superimposed on seasonal cycles are the variations associated with inter-annual and multi-decadal ocean-atmospheric oscillations. These oscillations are associated with anomalies in Sea Surface Temperature (SST), precipitation and wind patterns, leading to changes in water column stability and nutrient loading into the euphotic zone [17–19]. The El Niño-Southern Oscillation (ENSO), North Pacific Gyre Oscillation (NPGO), Indian Ocean Dipole (IOD) and Atlantic Multidecadal Oscillation (AMO) have all been shown to affect phytoplankton primary production [17–21]. These natural variations in water column conditions can cause a 10-fold variation in primary production between different regions, with low-nutrient subtropical waters at the lower end of production and highly eutrophic coastal regions at the upper end [22,23].

Given these natural variations in physico-chemical conditions and in phytoplankton primary production, it is expected that the physical changes associated with climate change will redistribute phytoplankton primary production. Over the past decades, increases in sea surface temperatures and ocean heat content, as well as enhanced precipitation relative to evaporation and sea ice melt, have caused significant variations in physico-chemical conditions of the water column [23,24]. Subsequent changes in temperature and density stratification, and nutrient loading into the euphotic zone are expected to affect phytoplankton growth and primary production under global climate change [23,24]. Several studies based on *in situ*, satellite and/or modelling observations have shown that changes in global primary production associated with climate change ranged from a 0.57-13% decrease [25–28] to a 2% increase [29]. Discrepancies between these estimates may be based on differences in methodology or in variations in temporal and spatial scales. It therefore seems that care has to be taken in estimating global primary production, especially considering that some regions will experience additional local forcing under climate change, such as melting of sea ice in polar regions. Overall, it is expected that primary production will decrease in temperate to tropical oceanic regions and will increase at high latitudes, while there is uncertainty on the direction, magnitude and differences of changing primary production in shelf and coastal regions [30].

One of the major challenges in estimating primary production from remote-sensing observations lies in the assignment of the photosynthetic efficiency of phytoplankton cells [31–33]. Models based on ocean-colour remote-sensing observations typically use a relationship between phytoplankton biomass and photosynthetic active radiation (PAR, 400-700 nm) to compute primary production [4,31,34,35]. One such relationship is the photosynthesis versus irradiance (P-I) curve, which can be represented by a variety of mathematical equations [36,37]. The initial slope (α^B) and the assimilation number (P_m^B) of the P-I curve may vary with environmental conditions such as irradiance, temperature and nutrient concentrations, as well as taxonomic composition and size structure of phytoplankton communities [33,38–43]. One of the strategies for the assignment of photosynthetic parameters in the computation of primary production on a global scale is to assign parameters on the basis of ecological provinces of the ocean [2,16,31,44,45], allowing for variations in photosynthetic parameters with season and with province. This strategy was adopted in the present study and an existing global database of P-I parameters [33] was extended to improve spatial and temporal coverage. The global P-I database was subsequently partitioned using Longhurst's geographical classification system of biomes and provinces [16]. The biogeographic classification is based on physical conditions that shape the structure and function of phytoplankton communities over large (basin) scales, and the supply of nutrients

and the average irradiance within the surface mixed layer that impact the physiological capacity of phytoplankton cells [16,33]. Another challenge in the estimation of primary production from satellite observations lies in the requirement to specify the vertical structure in phytoplankton biomass, given that the satellite observations are confined to a finite surface layer that is much smaller than the euphotic depth and is not resolved with depth. To overcome this limitation, we have used a large database of *in situ* chlorophyll-*a* profiles to extrapolate ocean-colour remote-sensing observations of surface chlorophyll-*a* through the water column [2,44,45]. Seasonal means of P-I parameters and chlorophyll-*a* profile parameters were then used together with a 20-year time series of remotely-sensed chlorophyll-*a* concentrations and surface PAR to establish global primary production and its changes over the two decades. The results are discussed in the context of the sensitivity of computed primary production to potential changes in the photosynthetic response of phytoplankton cells under changing environmental conditions.

2. Materials and Methods

2.1. Surface chlorophyll-a *data from satellites*

Surface chlorophyll-*a* concentrations at 9 km spatial resolution and monthly temporal resolution for the period of 1998-2018 were obtained from the European Space Agency (ESA) Ocean Colour Climate Change Initiative project (OC-CCIv4.1, https://esa-oceancolour-cci.org/). The dataset contains merged products of observations from the Sea-viewing Wide Field-of-View Sensor (SeaWiFS, 1997–2010), the MEdium Resolution Imaging Spectrometer (MERIS, 2002–2012), the Moderate Resolution Imaging Spectroradiometer (MODIS, 2002-present) and the Visible Infrared Imaging Radiometer Suite (VIIRS, 2012-present) that are climate-quality controlled, bias-corrected and error-characterized (see details below) [10].

2.2. Primary production model

Several models have been described to estimate primary production based on ocean-colour remote-sensing observations [29,35,46–48]. All models calculate daily water column production as a function of some measure of phytoplankton biomass and the photosynthetic response of phytoplankton to light. However, the different models can be categorised as linear or non-linear; spectral or non-spectral; vertically-uniform or vertically-non-uniform; or a combination of these [46,47]. They have also been categorised as depth-integrated or resolved and as wavelength-integrated or resolved [35]. Reducing models to a canonical form helps analyse similarities and differences between models and highlights the importance of model parameters [46,47,49]. The differences between spectral and non-spectral models are systematic and significant [47], but they can be corrected for [47,50,51]. In a study at the scale of the entire North Atlantic Ocean, Sathyendranath *et al.* [52] showed that ignoring the vertical structure in chlorophyll-*a* concentration reduced the computed primary production by about 9%, but in individual provinces, the difference could be higher (maximum reported value was about 16%). But the differences are systematic, and therefore, information on vertical structure should be taken into account when available. Furthermore, primary production within the deep chlorophyll maximum is likely fuelled by new production and would be important in calculations of new and export production [52].

In this study, we used a spectrally-resolved model that incorporates vertical structure in chlorophyll-*a* concentration [2,31,44,45,52], with recent updates [49]. This model simulates changes in photosynthesis as a function of irradiance using a two-parameter photosynthesis versus irradiance (P-I) function. The model has consistently performed well when compared with other models [5,35,53] and has been implemented on a global scale [2]. In the present study, considerable improvements have been made to the global coverage of the parameter database, while data provided by the Ocean Colour Climate Change Initiative (OC-CCI) project [10,54] allowed for the use of over 20 years of remote-sensing observations. The OC-CCI products [10] are multi-sensor products (reducing

missing data), in which biases between sensors have been corrected (avoiding artificial trends in data arising from systematic differences between biases) and have been processed with a common protocol for calculation of chlorophyll-*a* concentration (minimising any systematic differences arising from differences between algorithms). Melin et al. [55] have shown that the chlorophyll-*a* trends calculated with OC-CCI time series are consistent with those calculated from single sensor products, demonstrating the fitness of the data for climate change studies. All of these, along with the length of the time-series data, are key considerations when studying the variability in ocean primary production in the context of climate change. The model used here is identical to the one described in Sathyendranath *et al.* [49] (see Appendix A for a brief description of the steps involved), but with a notable improvement to the P-I parameter assignment, based on an enhanced *in situ* database.

2.3. Photosynthesis versus irradiance parameters

Parameters of the photosynthesis versus irradiance (P-I) curve were obtained from a global database [33,56] and additional literature sources [57–94]. A quality check was performed on all data (9,765 experiments) following Bouman *et al.* [33], using lower limits of the initial slope of the P-I curve α^B (0.002 mg C mg Chl-a^{-1} h^{-1} (μmol photons m^{-2} s^{-1})$^{-1}$) and the assimilation number P_m^B (0.2 mg C mg Chl-a^{-1} h^{-1}) and an upper limit for the maximum quantum yield of carbon fixation ϕ_m (0.15 mol C mol quanta^{-1}). The value of ϕ_m was calculated as α^B / $\bar{a}_B^*$ $\times$ 0.0231 [95] using α^B and either simultaneous measurements of the mean specific chlorophyll-*a* absorption coefficient $\bar{a}_B^*$ (in m^2 mg Chl-a^{-1}) or an estimate of $\bar{a}_B^*$ based on Brewin *et al.* [96,97] (see Appendix A). In addition, major outliers in the dataset were identified using the outermost fences of the Interquartile Range. After quality control, 8,676 experiments were used for further analysis. Note that this is a significant improvement over the P-I parameter database that was available at the time of Longhurst *et al.* [2], they had access to 1,862 P-I observations at that time, mostly from the North Atlantic Ocean.
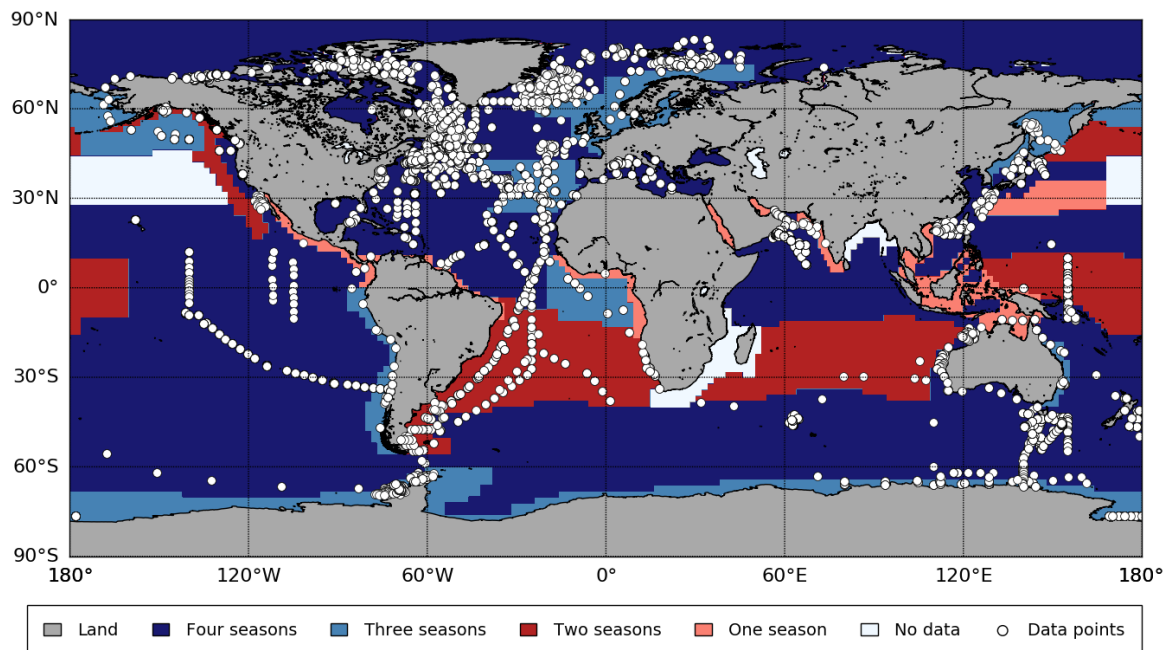
Figure 1. Sample locations for photosynthesis versus irradiance (P-I) experiments obtained from databases and literature with seasonal coverage in each biogeographic province as defined by Longhurst (2007). A total of 8,676 P-I experiments were used in the present study, covering 53 biogeographic provinces and 96.6% of the world's ocean. High seasonal data coverage was obtained for 37 provinces (3-4 seasons, 79.9% coverage).

To estimate regional primary production, P-I data were assigned to biogeographic provinces according to Longhurst [16] (Appendix B). The P-I database covered 53 provinces, representing 96.6% of the world's oceans (Figure 1). No *in situ* P-I experiments could be found for the coastal

areas of Africa (EAFR) and India (INDE) and two regions in the North Pacific Ocean (NPPF, NPSE).
The data were divided into seasons using 3-month intervals, i.e. March-May for spring/autumn,
June-August for summer/winter, September-November for autumn/spring and December-February
for winter/summer in the Northern/Southern Hemisphere. Mean and standard deviations of α^B
and P_m^B were calculated for each season and biogeographic province available in the P-I database
(Table 1). Temporal and spatial data gaps in α^B and P_m^B were filled by statistical analysis of the
relationships between seasons within each biogeographic province and the relationships between
adjacent biogeographic provinces (Figure 2). To this end, values of α^B and P_m^B were log-transformed and
significance ($p < 0.05$) was tested using ANOVA analysis followed by Tukey-Kramer post-hoc testing
for unequal sample sizes (Past 3, Hammer *et al.* 2001). Results were used to assign mean and standard
deviations of α^B and P_m^B for missing seasons and/or biogeographic provinces (Table 1) respecting
boundaries of the ocean basins and biomes [16]. Linear- and log-scaled mean values of α^B and P_m^B were
highly similar ($r^2 = 0.989$, $p < 0.001$; with the majority of data normally distributed on regional and
seasonal scales) and calculations of primary production were performed with linear-scaled mean and
standard deviations of each P-I parameter (Table 1) to support interpretation of (linear) trends in the
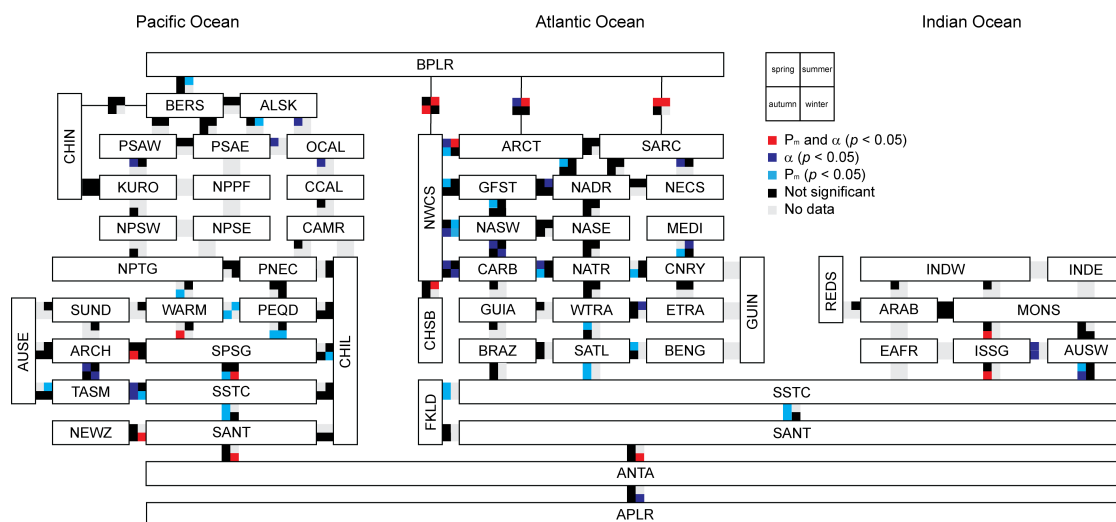sensitivity analyses (see below).

Figure 2. Relationships of photosynthesis versus irradiance (P-I) parameters between adjacent biogeographic
provinces. Seasonal relationships are indicated by colour blocks, with significant differences ($p < 0.05$) denoted for
the initial slope (α^B) and assimilation number (P_m^B) of the P-I curve (red), α^B only (dark blue) and P_m^B only (light
blue). Comparisons were not available for the coastal areas of Africa (EAFR) and India (INDE), two regions in the
North Pacific Ocean (NPPF, NPSE) and some seasons in other biogeographic regions due to lack of data (light grey).
Biogeographic provinces are listed in Appendix B.

2.4. Analyses of primary production

The sensitivity of primary production to changes in photosynthetic parameters was estimated using
three separate model runs for the period between 1998 and 2018, with three different P-I parameters
assignments as follows: a) with the mean of the P-I parameters for each of the provinces and seasons
(the main run); b) with the mean minus one standard deviation of the two P-I parameters (–1 SD); and c)
with the mean plus one standard deviation of the two P-I parameters (+1 SD) (Table 1). All other input
variables (i.e. light, chlorophyll-*a* and chlorophyll-*a* profile parameters) were kept the same for each of
these model runs. To assess the magnitude of change in primary production with change in individual
P-I parameters, an additional sensitivity analysis was performed for a sample year (arbitrarily chosen
to be 2003) in which either the initial slope (α^B) or the assimilation number (P_m^B) of the P-I curve was
adjusted by ± 1 standard deviation, while the other parameter was maintained at its mean value. In the
full model computations in which α^B and P_m^B were adjusted simultaneously, the relationship between
α^B and P_m^B, given by the light adaptation parameter (I_k in μmol photons m^{-2} s^{-1}), remained largely

unchanged. In the additional sensitivity analysis I_k was allowed to vary and increased for –1 SD α^B and +1 SD P_m^B and decreased for +1 SD α^B and –1 SD P_m^B. For all model computations, both annual and seasonal primary production rates were estimated on global and regional scales. Regions were selected based on Longhurst's definition of ocean basins (Antarctic, Atlantic, Indian and Pacific) and biomes (Coastal, Polar, Trades and Westerlies) [16].

Statistical analyses were used to assess relationships between P-I parameters and other (environmental) parameters available in the P-I database (latitude, depth, chlorophyll-*a*, PAR, temperature and nutrients; correlation and regression analysis), relationships between primary production estimates and input variables (chlorophyll-*a*, PAR and P-I parameters; correlation and regression analysis) and changes in primary production trends on various spatial and temporal scales (correlation analysis). To estimate the rate and direction of change in annual primary production between 1998-2018 for each grid point, monthly means were corrected for seasonality by subtracting monthly climatologies. The rate of change over time and its significance were calculated using linear regression and Student's *t* tests following Santer *et al.* [98]. Using the slope and intercept from the regression analysis, the percentage change per year in primary production (PP) was calculated as $100 \cdot ((12 \cdot slope) / (intercept + PP_{climatology}))$. Before all statistical procedures, data were tested for normality and homogeneity of variances and transformed for further statistical analysis when necessary. Differences were considered significant when $p < 0.05$.

The impact of different climate indices on global and regional primary production was characterised based on annual mean anomalies that were corrected for seasonality following Racault *et al.* [19]. Student's *t* tests were used to assess statistical significance of the relationships considering autocorrelations of the time series following Santer *et al.* [98]. Climate indices were obtained from the National Oceanic and Atmospheric Administration (NOAA) (www.esrl.noaa.gov/psd/data/climateindices/), Kao and Yu [99] (www.ess.uci.edu/ yu/2OSC/) and Di Lorenzo *et al.* [17] (www.o3d.org/npgo/).

Table 1. Sample size (n), mean and standard deviation (SD) of the initial slope (α^B in mg C mg Chl-a^{-1} h^{-1} μmol photons m^{-2} s^{-1}) and the assimilation number (P_m^B in mg C mg Chl-a^{-1} h^{-1}) of the photosynthesis versus irradiance (P-I) curve for each biogeographic province and season. Values in blue are obtained from statistical comparisons between seasons and biogeographic provinces, while other values are directly obtained from the P-I database. Biogeographic provinces are listed in Appendix B.

BIOME/BASIN	PROV	Spring α^B n	Mean	SD	P_m^B n	Mean	SD	Summer α^B n	Mean	SD	P_m^B n	Mean	SD	Autumn α^B n	Mean	SD	P_m^B n	Mean	SD	Winter α^B n	Mean	SD	P_m^B n	Mean	SD
Coastal																									
Atlantic	NECS	18	0.020	0.005	18	3.25	0.64	12	0.022	0.007	15	2.83	1.62	30	0.021	0.006	1	2.22		30	0.021	0.006	34	3.04	1.18
	CNRY	1	0.035		1	4.00		33	0.022	0.006	34	3.92	1.56	11	0.026	0.005	34	4.08	1.70	1	0.016		3	3.30	1.13
	GUIN	1	0.012		1	1.50		48	0.017	0.008	50	1.68	1.04	20	0.017	0.006	19	1.68	0.62	48	0.017	0.008	50	1.68	1.04
	GUIA	77	0.024	0.017	34	2.52	1.88	109	0.023	0.016	56	2.71	1.90	2	0.024	0.008	2	2.71	1.35	109	0.023	0.016	6	2.90	1.21
	NWCS	495	0.031	0.020	515	2.49	1.18	259	0.024	0.017	260	3.23	1.47	335	0.044	0.021	332	3.58	1.66	121	0.037	0.018	125	2.85	1.36
	CHSB	41	0.036	0.018	41	3.29	1.46	35	0.016	0.013	36	2.04	1.66	18	0.041	0.018	19	4.80	1.43	59	0.038	0.018	96	3.12	1.82
	BRAZ	9	0.029	0.016	10	2.22	1.82	48	0.017	0.008	15	2.69	1.95	5	0.014	0.005	5	3.63	2.05	48	0.017	0.008	15	2.69	1.95
	FKLD	28	0.017	0.009	31	1.68	1.24	48	0.017	0.008	50	1.68	1.04	20	0.017	0.006	19	1.68	0.62	48	0.017	0.008	50	1.68	1.04
	BENG	2	0.044	0.000	4	4.24	2.52	25	0.027	0.012	26	3.66	1.67	23	0.026	0.011	22	3.56	1.52	25	0.027	0.012	26	3.66	1.67
Indian	EAFR	117	0.027	0.009	101	4.76	1.66	32	0.030	0.009	17	5.36	1.07	285	0.027	0.011	6	3.43	1.27	280	0.027	0.010	203	4.38	1.62
	REDS	46	0.013	0.007	85	3.29	1.36	4	0.022	0.006	4	4.13	2.07	117	0.027	0.009	101	4.76	1.66	32	0.030	0.009	17	5.36	1.07
	ARAB	13	0.034	0.010	98	4.00	1.48	114	0.024	0.011	81	3.72	1.40	117	0.027	0.009	101	4.76	1.66	32	0.033	0.009	17	5.36	1.07
	INDE	65	0.042	0.021	62	3.39	2.13	5	0.034	0.028	7	4.10	1.53	56	0.034	0.018	56	2.97	1.89	6	0.039	0.015	6	2.50	1.01
	INDW	9	0.033	0.027	6	3.43	1.27	114	0.024	0.011	64	3.94	1.70	117	0.027	0.009	35	3.65	1.48	32	0.030	0.009	29	4.29	1.91
	AUSW	56	0.034	0.018	56	2.97	1.89	6	0.039	0.015	6	2.50	1.01	56	0.047	0.019	56	3.38	2.21	19	0.028	0.017	3	4.05	0.80
Pacific	ALSK	7	0.029	0.012	8	3.91	0.89	61	0.026	0.020	35	4.67	1.90	23	0.023	0.011	43	4.53	1.77	51	0.025	0.010	43	4.53	1.77
	CCAL	42	0.038	0.023	53	3.80	1.76	9	0.012	0.007	26	4.17	1.91	11	0.008	0.001	28	3.21	1.47	2	0.016	0.006	20	1.70	1.08
	CAMR	1	0.026		2	1.50	0.20	31	0.020	0.009	26	4.17	1.91	18	0.026	0.014	28	3.21	1.47	2	0.016	0.006	28	3.48	2.22
	CHIL	8	0.032	0.011	7	2.50	0.93	79	0.031	0.012	78	2.35	1.36	33	0.029	0.010	89	2.35	1.35	4	0.016	0.016	4	2.10	2.12
	CHIN	25	0.026	0.007	17	5.48	1.72	31	0.020	0.009	22	3.59	1.99	18	0.026	0.014	10	4.48	3.23	2	0.016	0.006	2	4.55	1.34
	SUND	26	0.025	0.010	20	4.10	2.30	12	0.041	0.018	16	3.43	2.13	67	0.031	0.012	68	2.85	1.51	11	0.029	0.014	12	2.55	2.13
	AUSE	19	0.050	0.020	320	4.41	1.53	4	0.050	0.018	4	4.65	3.15	31	0.047	0.019	15	2.53	2.13	8	0.042	0.018	11	1.75	0.94
	NEWZ	8	0.045	0.013	9	4.48	1.46	23	0.021	0.011	22	4.63	1.51	9	0.036	0.009	8	3.70	1.42	2	0.044	0.003	2	3.30	0.28
Polar																									
Antarctic	ANTA	1	0.007		2	1.01	0.92	41	0.018	0.009	75	1.27	0.50	12	0.021	0.005	9	1.58	0.72	54	0.019	0.008	11	1.48	0.74
	APLR	52	0.035	0.009	67	1.66	0.92	268	0.029	0.014	340	1.89	1.26	140	0.026	0.009	162	1.86	0.90	54	0.019	0.008	569	1.86	1.13
Atlantic	BPLR	141	0.031	0.016	154	2.03	0.83	542	0.030	0.017	572	1.67	0.99	189	0.024	0.013	192	1.65	0.84	21	0.031	0.019	21	1.85	0.78
	ARCT	278	0.039	0.017	329	2.38	1.07	298	0.036	0.016	313	2.24	0.99	39	0.032	0.018	59	2.18	0.78	27	0.028	0.013	27	2.38	0.85
	SARC	116	0.044	0.017	126	2.74	1.09	89	0.041	0.014	92	2.59	1.27	206	0.043	0.016	2	1.40	0.46	206	0.043	0.016	220	2.66	1.17
Pacific	BERS	7	0.029	0.012	8	3.26	1.81	21	0.024	0.007	22	2.85	1.18	23	0.023	0.011	25	2.41	1.39	51	0.025	0.010	55	2.71	1.38
Trades																									
Atlantic	NATR	15	0.025	0.015	14	3.60	1.76	165	0.035	0.021	165	2.85	1.84	27	0.027	0.011	26	2.52	2.40	6	0.032	0.018	7	5.23	1.60
	WTRA	16	0.013	0.007	16	3.06	2.18	109	0.023	0.016	6	2.90	1.21	32	0.025	0.019	34	2.52	21.88	109	0.023	0.016	56	2.71	1.90
	ETRA	4	0.037	0.026	4	2.90	3.23	62	0.016	0.016	61	3.01	1.79	6	0.024	0.014	6	2.97	1.06	52	0.025	0.016	51	3.02	1.76
	SATL	77	0.024	0.017	77	1.99	1.37	109	0.023	0.016	109	1.87	1.35	32	0.020	0.014	32	1.59	1.28	109	0.023	0.016	109	1.87	1.35
	CARB	22	0.010	0.005	21	3.20	1.99	16	0.023	0.010	2	6.25	0.92	25	0.028	0.012	16	5.73	1.79	28	0.022	0.009	28	3.48	2.22
Indian	MONS	5	0.028	0.005	64	3.94	1.70	9	0.024	0.007	64	3.94	1.70	40	0.022	0.007	35	3.65	1.48	35	0.027	0.006	29	4.29	1.91
	ISSG	10	0.007	0.003	10	1.94	1.61	14	0.007	0.003	6	2.50	1.01	4	0.009	0.002	26	2.86	1.31	14	0.007	0.003	3	4.05	0.80
Pacific	NPTG	3	0.013	0.008	9	4.97	0.66	8	0.015	0.003	6	4.39	2.12	10	0.017	0.006	18	4.79	1.70	7	0.016	0.004	26	4.88	0.74
	PNEC	2	0.031	0.011	9	3.46	1.49	12	0.017	0.006	15	3.94	1.85	11	0.017	0.004	27	3.54	1.74	27	0.018	0.005	3	1.75	0.77
	PEQD	11	0.017	0.004	18	4.85	1.58	27	0.018	0.005	6	3.79	1.04	27	0.018	0.005	8	4.76	0.97	16	0.019	0.005	17	4.39	1.33
	WARM	163	0.030	0.015	160	2.23	1.31	220	0.031	0.016	221	2.16	1.28	220	0.031	0.016	221	2.16	1.28	57	0.033	0.020	61	1.97	1.19
	ARCH	67	0.031	0.012	68	2.85	1.51	11	0.029	0.014	12	2.55	2.13	26	0.025	0.010	20	4.10	2.30	19	0.028	0.017	22	2.81	1.92
Westerlies																									
Antarctic	SSTC	18	0.021	0.016	47	4.12	2.01	45	0.034	0.011	83	2.25	1.56	33	0.029	0.010	53	4.42	1.39	4	0.016	0.016	5	5.30	1.57
	SANT	3	0.026	0.002	28	1.85	0.42	41	0.023	0.006	136	1.58	0.53	10	0.027	0.003	18	1.99	0.54	55	0.023	0.006	242	1.62	0.54
Atlantic	NADR	47	0.032	0.014	42	3.32	1.25	4	0.051	0.023	4	3.03	0.73	49	0.025	0.014	52	2.14	1.20	7	0.036	0.007	7	2.83	0.45
	GFST	50	0.034	0.012	47	4.39	1.60	14	0.013	0.006	13	2.40	1.99	24	0.040	0.016	28	3.08	1.67	7	0.054	0.020	7	4.32	2.06
	NASW	137	0.031	0.018	96	3.84	2.53	113	0.029	0.021	92	2.13	1.85	65	0.036	0.024	57	4.09	2.23	33	0.041	0.019	30	4.66	1.35
	MEDI	46	0.013	0.007	85	3.29	1.36	26	0.005	0.003	36	2.65	1.86	77	0.032	0.021	113	2.57	1.66	55	0.040	0.019	105	2.64	1.35
	NASE	25	0.029	0.018	27	3.95	1.78	17	0.030	0.009	17	2.72	1.67	44	0.025	0.014	60	2.86	2.01	86	0.031	0.018	7	5.23	1.60
Pacific	PSAE	18	0.035	0.014	18	2.48	0.74	42	0.032	0.013	46	2.54	0.81	8	0.025	0.012	9	2.35	1.06	68	0.032	0.013	73	2.50	0.82
	PSAW	33	0.039	0.011	31	3.32	0.93	8	0.036	0.018	8	3.51	1.55	41	0.038	0.013	39	3.36	1.06	41	0.038	0.013	39	3.36	1.06
	KURO	83	0.020	0.009	81	3.62	1.64	61	0.017	0.007	60	2.88	1.41	82	0.020	0.007	86	3.62	1.70	10	0.021	0.009	9	4.63	0.52
	NPPF	134	0.027	0.013	144	3.28	1.46	111	0.024	0.013	114	2.79	1.23	96	0.020	0.008	100	3.48	1.65	10	0.021	0.009	9	4.63	0.52
	NPSE	134	0.027	0.013	144	3.28	1.46	111	0.024	0.013	114	2.79	1.23	96	0.020	0.008	100	3.48	1.65	10	0.021	0.009	9	4.63	0.52
	NPSW	83	0.020	0.009	81	3.62	1.64	61	0.017	0.007	60	2.88	1.41	6	0.015	0.005	5	3.22	0.59	10	0.021	0.009	9	4.63	0.52
	OCAL	10	0.007	0.002	10	1.87	0.59	12	0.017	0.006	6	4.26	0.81	1	0.006		9	2.35	1.06	10	0.021	0.009	73	2.50	0.82
	TASM	8	0.053	0.017	12	5.10	1.51	19	0.053	0.013	25	4.68	2.04	3	0.029	0.001	19	5.99	1.54	12	0.053	0.012	13	4.52	1.22
	SPSG	240	0.021	0.015	246	1.79	1.33	27	0.022	0.011	29	1.35	0.79	3	0.029	0.001	281	1.77	1.30	4	0.025	0.004	6	3.16	1.37

3. Results

3.1. Global and regional annual primary production

Global annual primary production computed using mean photosynthesis versus irradiance (P-I) parameters (for each biogeographic province and for each season) varied from 38.8 to 42.1 Gt C y^{-1} in the period 1998-2018 (Table 2; Figures 3, 4A). Summer (11.6-12.9 Gt C) was the most productive season in each of the years, followed by spring (11.0-11.8 Gt C), autumn (8.7-9.5 Gt C per season) and winter (7.5-8.0 Gt C per season) (Figure 4B). On regional scales, annual primary production was highest in the Pacific Ocean (43.4-44.6%), followed by the Atlantic (27.7-28.8%), Indian (16.0-17.0%) and Antarctic Oceans (10.7-11.6%) (Table 2; Figure 3). In addition, the highest annual primary production rates were found at low latitudes in the Trades biome (39.6-41.1%), followed by the Westerlies (29.0-30.6%), Coastal (22.6-24.7%) and Polar biomes (5.9-6.8%) (Table 2; Figure 3). These regional differences in

annual primary production were related to the surface area of the specific ocean basins and biomes (r^2 = 0.643, p < 0.01), with the coastal regions being relatively more and polar regions relatively less productive than the other regions when computed as a rate per unit area (Table 2; Figure 3A).

Table 2. Climatological mean and standard deviation (n = 21) of annual primary production (in Gt C y^{-1}) between 1998-2018 for each ocean basin and biome as defined by Longhurst (2007). Range in annual primary production between 1998-2018 is given in parenthesis. Results are given for primary production estimates based on mean, -1 standard deviation and +1 standard deviation photosynthesis versus irradiance (P-I) parameters. Surface areas (in km^2) for each ocean basin and biome are also provided.

		Coastal $47 \cdot 10^6$	Polar $57 \cdot 10^6$	Trades $141 \cdot 10^6$	Westerlies $131 \cdot 10^6$	Total $376 \cdot 10^6$
Mean P-I						
Antarctic	$79 \cdot 10^6$		0.77±0.07 (0.64-0.87)		3.76±0.10 (3.60-3.99)	4.53±0.14 (4.27-4.75)
Atlantic	$94 \cdot 10^6$	2.58±0.16 (2.36-2.78)	1.12±0.06 (1.02-1.27)	5.32±0.13 (5.07-5.49)	2.45±0.04 (2.38-2.54)	11.48±0.33 (10.90-11.92)
Indian	$48 \cdot 10^6$	3.12±0.17 (2.88-3.36)		3.60±0.11 (3.37-3.75)		6.71±0.26 (6.24-7.11)
Pacific	$155 \cdot 10^6$	3.97±0.21 (3.59-4.22)	0.71±0.04 (0.62-0.79)	7.42±0.27 (6.87-7.74)	5.84±0.13 (5.67-5.99)	17.94±0.54 (16.98-18.64)
Total	$376 \cdot 10^6$	9.67±0.51 (8.92-10.35)	2.61±0.14 (2.30-2.83)	16.33±0.44 (15.41-16.76)	12.05±0.23 (11.72-12.48)	40.66±1.19 (38.79-42.07)
Mean P-I -1 standard deviation		Coastal $47 \cdot 10^6$ km^2	Polar $57 \cdot 10^6$	Trades $141 \cdot 10^6$	Westerlies $131 \cdot 10^6$	Total $376 \cdot 10^6$
Antarctic	$79 \cdot 10^6$		0.41±0.03 (0.35-0.46)		2.19±0.06 (2.09-2.33)	2.59±0.08 (2.45-2.74)
Atlantic	$94 \cdot 10^6$	1.35±0.08 (1.23-1.46)	0.59±0.03 (0.54-0.65)	2.09±0.06 (1.98-2.17)	1.18±0.02 (1.15-1.22)	5.21±0.16 (4.94-5.42)
Indian	$48 \cdot 10^6$	1.85±0.10 (1.72-1.99)		2.18±0.06 (2.04-2.27)		4.03±0.15 (3.76-4.26)
Pacific	$155 \cdot 10^6$	1.93±0.10 (1.73-2.05)	0.40±0.02 (0.35-0.44)	4.13±0.15 (3.81-4.32)	3.15±0.07 (3.01-3.24)	9.61±0.29 (9.10-9.97)
Total	$376 \cdot 10^6$	5.13±0.26 (4.72-5.48)	1.39±0.07 (1.25-1.51)	8.40±0.24 (7.89-8.62)	6.52±0.13 (6.33-6.76)	21.45±0.63 (20.43-22.21)
Mean P-I +1 standard deviation		Coastal $47 \cdot 10^6$	Polar $57 \cdot 10^6$	Trades $141 \cdot 10^6$	Westerlies $131 \cdot 10^6$	Total $376 \cdot 10^6$
Antarctic	$79 \cdot 10^6$		1.10±0.11 (0.90-1.24)		5.24±0.13 (5.03-5.56)	6.33±0.20 (5.95-6.63)
Atlantic	$94 \cdot 10^6$	3.78±0.23 (3.45-4.06)	1.66±0.10 (1.50-1.89)	8.43±0.20 (8.05-8.70)	3.69±0.06 (3.59-3.83)	17.57±0.50 (16.69-18.24)
Indian	$48 \cdot 10^6$	4.35±0.24 (4.01-4.69)		4.95±0.15 (4.63-5.15)		9.30±0.37 (8.64-9.85)
Pacific	$155 \cdot 10^6$	5.94±0.31 (5.39-6.32)	1.02±0.06 (0.89-1.13)	10.60±0.38 (9.86-11.06)	8.39±0.18 (7.99-8.61)	25.94±0.79 (24.56-26.97)
Total	$376 \cdot 10^6$	14.07±0.75 (12.98-15.07)	3.77±0.22 (3.31-4.10)	23.98±0.64 (22.71-24.61)	17.31±0.33 (16.83-17.93)	59.14±1.73 (56.49-61.20)

3.2. Trends in primary production

Linear trends in annual primary production between 1998 and 2018 varied considerably on regional scales (Figure 3B). At low and mid latitudes, trends in primary production were generally weak and negative (up to -3.0%), although large areas of positive trends were also observed in the South Atlantic Ocean and the South Pacific Ocean. In polar and coastal (upwelling) regions, stronger, positive trends in primary production were observed (up to +4.5%). Although significant linear trends were observed at individual pixels, the observed inter-annual changes in primary production on global and regional scales did not follow a linear pattern.

Inter-annual trends in global primary production showed an increase in rates between 1998 and 2003, relatively stable rates between 2003 and 2011 and a subsequent decrease in rates until 2015 after which rates showed a minor increase (Figure 4A). Annual primary production in the Atlantic and Pacific Oceans showed similar inter-annual trends to global primary production (r^2 = 0.866, 0.926, p < 0.001) (Figure 4C). Trends in annual primary production in the other ocean basins varied from the global trend, with relatively lower production between 2003-2011 in the Antarctic Ocean (r^2 = 0.675, p < 0.001) and a relatively early decrease in production in the Indian Ocean (r^2 = 0.828, p < 0.001) (Figure 4C). Annual primary production in the Coastal, Trades and Westerlies biomes showed inter-annual trends comparable with that in global primary production (r^2 = 0.815-0.856, p < 0.001) with the highest rates observed between 1998 and 2000 in the Trades biome and a relatively slow increase in production between 1998 and 2011 in the Westerlies biome (Figure 4E). In the Polar biome, production decreased relatively early between 2004 and 2011 and was relatively high after 2015 compared with trends for global annual primary production (r^2 = 0.510, p < 0.001).
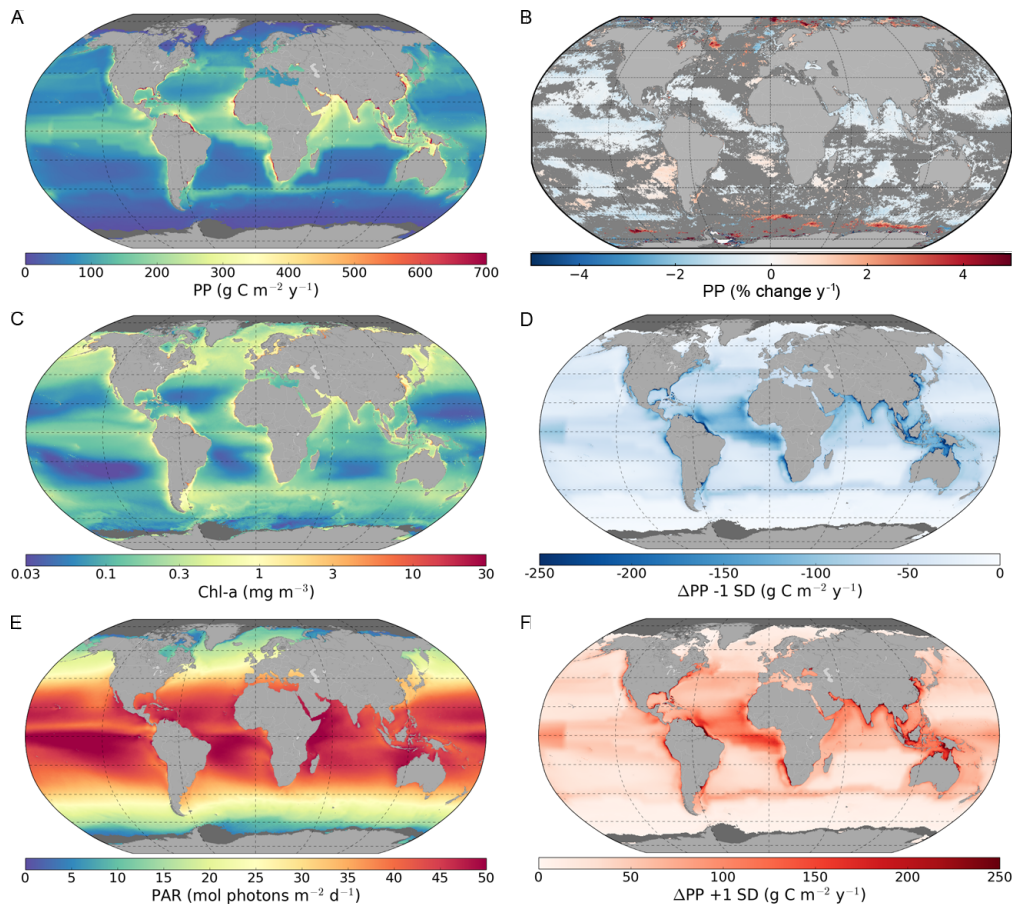
Figure 3. Maps of global annual primary production (PP) and associated parameters for the period of 1998-2018. A) Global annual primary production based on mean photosynthesis versus irradiance (P-I) parameters, B) Linear trends in global annual primary production between 1998-2018 given as percentage change per year (dark grey colour represents non-significant trends), C) Remote-sensing derived mean surface chlorophyll-*a* (Chl-a), D) Difference in primary production between mean P-I parameters and -1 standard deviation (-1 SD) based estimations, E) Remote-sensing derived Photosynthetic Active Radiation (PAR, 400-700 nm), and F) Difference in primary production between mean P-I parameters and +1 standard deviation (+1 SD) based estimations.

Trends in seasonal global primary production were highest in late spring to mid-summer with the lowest rates observed in December for the Northern Hemisphere and in June for the Southern Hemisphere (Figure 4B). Most regions showed similar seasonal trends in primary production with the peak occurring either earlier (Pacific Ocean and Westerlies and Coastal biomes) or later (Antarctic and Atlantic Oceans and Polar biome) in summer (r^2 = 0.782-0.962, $p < 0.001$) (Figure 4D,F). Monthly primary production in the Trades biome was more variable from spring to autumn compared with the global trend (r^2 = 0.782, $p < 0.01$) (Figure 4D). Trends in seasonal primary production in the Indian Ocean deviated most from the global trend, with two peaks in monthly primary production observed in spring and autumn and the lowest rates observed in summer (Figure 4F).

Inter-annual and seasonal trends in global primary production were closely related to chlorophyll-*a* biomass (Spearman's Rank Correlation coefficient r_s = 0.742-0.939, $p < 0.05$) (Figure 3C). In the Antarctic and Indian Oceans and Trades biome, annual primary production was also related to PAR (r_s = 0.484-0.600, $p < 0.05$) (Figure 3E). The variations in global primary production were associated with trends in the El Niño-Southern Oscillation (ENSO) (Multivariate ENSO Index (MEI), r = -0.389; ENSO Eastern Pacific (EP) index, r = -0.419) and the Atlantic Multidecadal Oscillation (AMO) (r = 0.304). The initial increase in global annual primary production between 1998-2003 was related to ENSO (EP index, r = -0.953), AMO (r = 0.973) and the Indian Ocean Dipole (IOD) (r = 0.551), while the decrease in global annual primary production after 2011 was related to ENSO (MEI, r = -0.716; ENSO Central Pacific (CP) index, r = -0.902) and the Pacific Decadal Oscillation (r = -0.861).
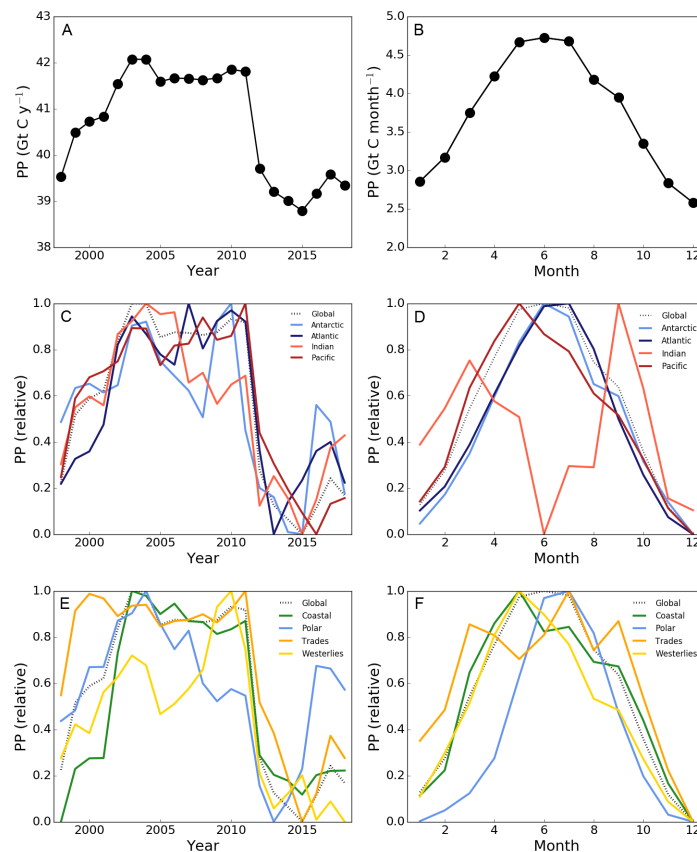
Figure 4. Trends in primary production (PP) with A) Annual global primary production for each year in the period between 1998-2018, B) Mean monthly primary production, C) Relative annual and D) Monthly primary production for each oceanic basin and E) Relative annual and F) monthly primary production for each biome as defined by Longhurst (2007). The dotted lines illustrate the relative global primary production per year (C,E) and month (D,F). Estimates of monthly primary production for the Southern Hemisphere were shifted to depict the summer season (December-February) along with that of the Northern Hemisphere (June-August) in months 6-8. Relative trends for each basin and biome were calculated by subtracting the minimum PP from the annual (C,E) or monthly (D,F) PP and dividing this by the difference between the minimum and maximum PP between 1998-2018 or between January-December.

3.3. Sensitivity of primary primary production to changes in photosynthetic parameters

Global annual primary production varied from 20.4 to 22.2 Gt C y^{-1} between 1998 and 2018 when both P-I parameters were reduced simultaneously by one standard deviation (–1 SD), whereas the values ranged from 56.5 to 61.2 Gt C y^{-1} when the P-I parameters were increased by one standard deviation (+1 SD) (–46.5% and +44.9% compared with the results using the mean P-I estimates) (Table 2; Figures 3D, 3F, 5). The magnitude of the decrease in primary production when the P-I parameters were adjusted by –1 standard deviation was always greater than the increase in production when the P-I parameters were adjusted by +1 standard deviation (Figure 5). The sensitivity of primary production to changes in P-I parameters was highest in the Atlantic Ocean, followed by the Pacific, Antarctic and Indian Oceans (Figures 3D, 3F, 5; Table 2). The sensitivity was highest in the Trades biome and lowest in the Westerlies biome (Figures 3D, 3F, 5; Table 2). Trends in global and regional annual primary production for the sensitivity analyses (data not shown) were similar to those observed for the main model run with mean P-I parameters (Table 2; Figures 3B, 4) ($r^2 = 0.978$-0.999, $p < 0.001$).

On a seasonal basis, global primary production changed between –50.1 to –43.7% and +42.0 to +48.6% when the photosynthetic parameters were adjusted by –1 and +1 standard deviation, respectively (Figure 5). The highest deviation from the mean P-I based primary production estimates was observed during spring and summer in the Atlantic Ocean and in the Trades biome, whereas the lowest deviation was observed during autumn and winter in the Antarctic Ocean and Westerlies biome.

289 Trends in seasonal primary production were similar to those observed for the mean photosynthetic
290 parameters estimates (Figure 4) when the photosynthetic parameters were adjusted by +1 standard
291 deviation (data not shown). When the photosynthetic parameters were adjusted by −1 standard
292 deviation, seasonal trends changed in the Indian Ocean and Coastal and Trades biomes. Primary
293 production in these regions became relatively lower in spring and summer compared with other
294 seasons (data not shown). No changes in seasonal primary production trends were observed in
295 the Antarctic, Atlantic and Pacific Oceans and Polar and Westerlies biomes when photosynthetic
296 parameters were adjusted by −1 standard deviation.
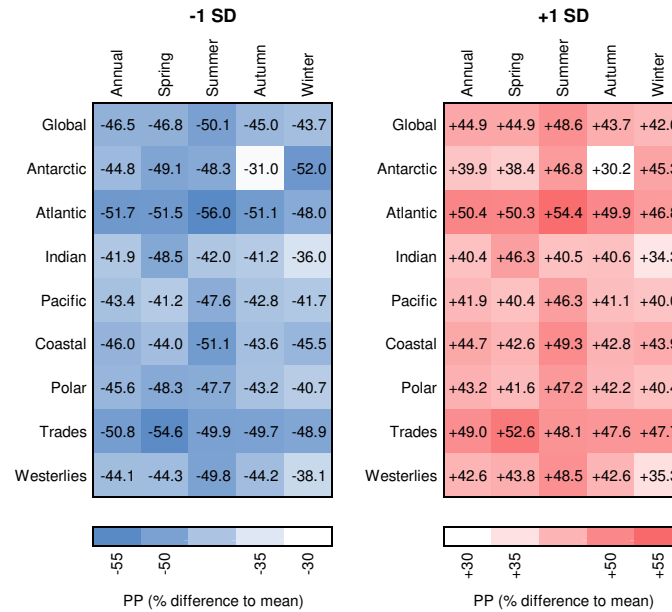
Figure 5. Percentage change in primary production (PP) for estimates based on mean photosynthesis versus irradiance (P-I) parameters ±1 standard deviation compared with estimates based on mean P-I parameters. Mean percentage differences in annual and seasonal primary production for each ocean basin and biome are given. Data was obtained from model computations in which both P-I parameters were adjusted simultaneously and the light adaptation parameter (I_k) was unchanged.

297 *3.4. Relationship between photosynthetic parameters and primary production*

298 It was expected that the changes in the magnitude of global and regional primary production were
299 driven by variations in photosynthetic parameters as all other input variables remained unchanged
300 between the different model computations. When the relative change in primary production was
301 compared with that of the P-I parameters for −1 SD and +1 SD estimates, variations were shown to be
302 closely coupled (the light adaptation parameter I_k was unchanged) (Figure 6). Both the initial slope of
303 the P-I curve (α^B) ($r^2 = 0.490$ for −1 SD and $r^2 = 0.508$ for +1 SD estimates) and the assimilation number
304 (P_m^B) ($r^2 = 0.750$ for −1 SD and $r^2 = 0.719$ for +1 SD estimates) showed positive linear relationships
305 with primary production for each season and biogeographic province. The weaker sensitivity of
306 daily, water column primary production to change in α^B, relative to that of P_m^B, could be explained
307 by the importance of α^B under light-limited conditions, as opposed to P_m^B whose effect is dominant
308 at light-saturating conditions. It is important to note that the ratio of P_m^B to α^B (i.e. I_k) remained
309 unchanged between these different estimates of primary production. Independent variations in α^B
310 and P_m^B that modify I_k could lead to higher sensitivity of primary production to the change [100–103].
311 The sensitivity analysis in which α^B and P_m^B were independently adjusted by ±1 standard deviation
312 (variable I_k) showed that changes in P_m^B caused greater variation in global annual primary production
313 than changes in α^B (Figure 7). Significant relationships between P-I parameters and primary production
314 were also observed when α^B and P_m^B were varied independently (−1 SD α^B: $y = 0.570\,x$, $r^2 = 0.836$; +1
315 SD α^B: $y = 0.322\,x$, $r^2 = 0.440$; −1 SD P_m^B: $y = 0.741\,x$, $r^2 = 0.908$; +1 SD P_m^B: $y = 0.492\,x$, $r^2 = 0.733$).

316 When I_k increased (–1 SD α^B and +1 SD P_m^B), primary production became more sensitive to changes in
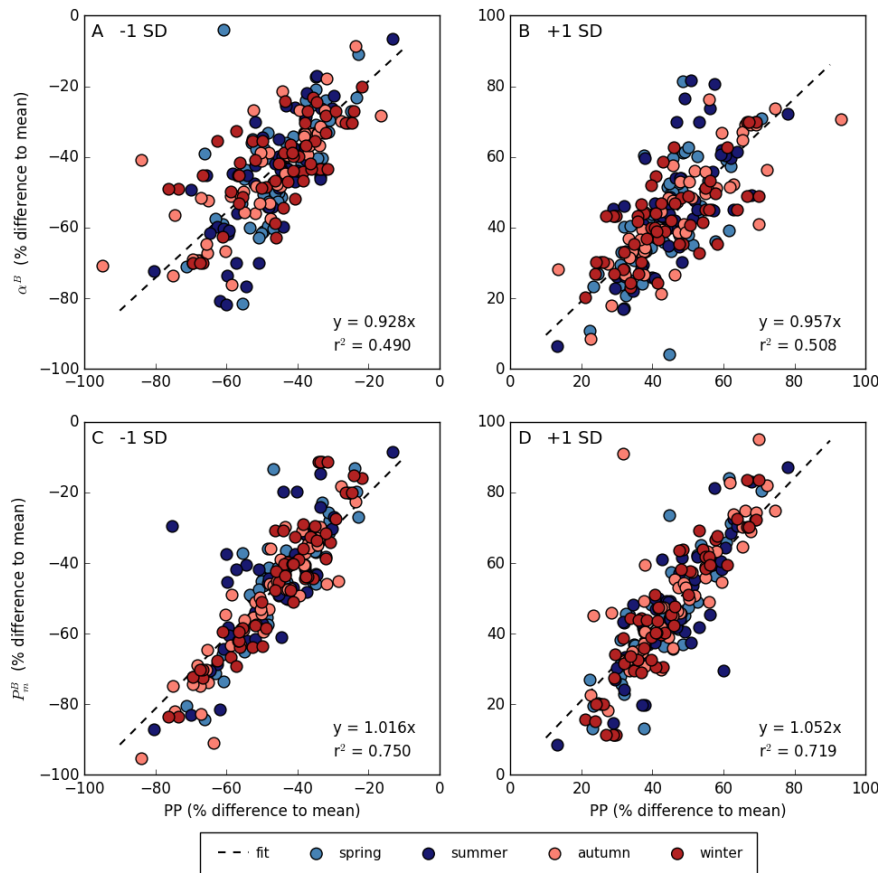317 P_m^B compared with those in α^B (see slope of relationships above).

Figure 6. Relationship between photosynthesis versus irradiance (P-I) parameters and primary production (PP) expressed as percentage difference in A,B) the initial slope (α^B) and C,D) the assimilation number (P_m^B) of the P-I curve and primary production (PP) for -1 standard deviation (A,C) and +1 standard deviation (B,D) compared with mean P-I parameters estimates. Each point represents a biogeographic province and season for the period between 1998-2018.
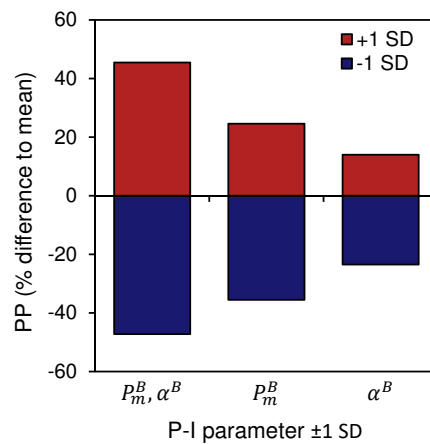
Figure 7. Percentage change in global annual primary production (PP) compared with estimates based on mean photosynthesis versus irradiance (P-I) parameters. Results from three different sensitivity analysis are given: 1) Both the initial slope (α^B) and assimilation number (P_m^B) of the P-I curve were adjusted by ± 1 standard deviation (SD) [P_m^B, α^B], 2) Only P_m^B was adjusted by ± 1 standard deviation [P_m^B], and 3) Only α^B was adjusted by ± 1 standard deviation [α^B].

3.5. Variation in photosynthetic parameters

In the global P-I parameter database α^B ranged between 0.002-0.085 mg C mg Chl-a^{-1} h^{-1} (μmol photons m^{-2} s^{-1})$^{-1}$ and P_m^B between 0.20-8.00 mg C mg Chl-a^{-1} h^{-1}. Mean values for each biogeographic province ranged between 0.005 and 0.054 mg C mg Chl-a^{-1} h^{-1} (μmol photons m^{-2} s^{-1})$^{-1}$ for α^B and between 1.01 and 6.25 mg C mg Chl-a^{-1} h^{-1} for P_m^B (Table 1). Lowest mean values of α^B and P_m^B were observed in the Mediterranean (MEDI, summer) and Antarctic (ANTA, spring) provinces, whereas the highest values were observed in the Gulf Stream (GFST, winter) and Caribbean (CARB, summer) provinces, respectively (Table 1). Standard deviations varied between 0.2 and 99.1% (average of 43.8%) for α^B and between 8.6 and 111.6% (average of 47.1%) for P_m^B (Table 1). Similar to observations reported in Bouman *et al.* [33], spatial and temporal variations in photosynthetic parameters could be related to local environmental conditions. Relationships between α^B and environmental conditions were variable between ocean basins and biomes resulting in relative weak relationships on a global scale (Figure 8). The initial slope α^B increased with daily photosynthetic active radiation (PAR) in the Atlantic and Indian Oceans and with nitrate concentrations in the Antarctic, Atlantic and Pacific Oceans (Figure 8). Positive relationships between α^B and chlorophyll-*a* were observed at mid latitudes (Trades biome), but a negative relationship was observed in the Coastal biome. The standard deviation of α^B increased at lower levels of PAR, at lower nitrate and silicate concentrations and at higher chlorophyll-*a* concentrations, but no other significant relationships with environmental parameters were observed (Figure 8). The assimilation number P_m^B showed overall stronger relationships with environmental conditions compared with α^B (Figure 8). Notably, P_m^B increased with temperature and PAR, possibly coinciding with latitudinal differences (Figure 8). The Pacific Ocean deviated from these results with an opposite trend observed between P_m^B and temperature at higher latitudes (data not shown). A negative relationship was observed between P_m^B and depth in all ocean basins and biomes, consistent with the known decline in P_m^B with decreasing temperature and light. P_m^B was generally lower at low phosphate concentrations, with strongest relationships observed in the Antarctic, Atlantic and Indian Oceans at higher latitudes in the Polar and Coastal biomes. Variation in P_m^B as expressed by the standard deviation increased at higher temperatures and lower latitudes (Figure 8). The standard deviation of P_m^B also showed a positive relationship with depth and negative relationships with nutrient conditions.
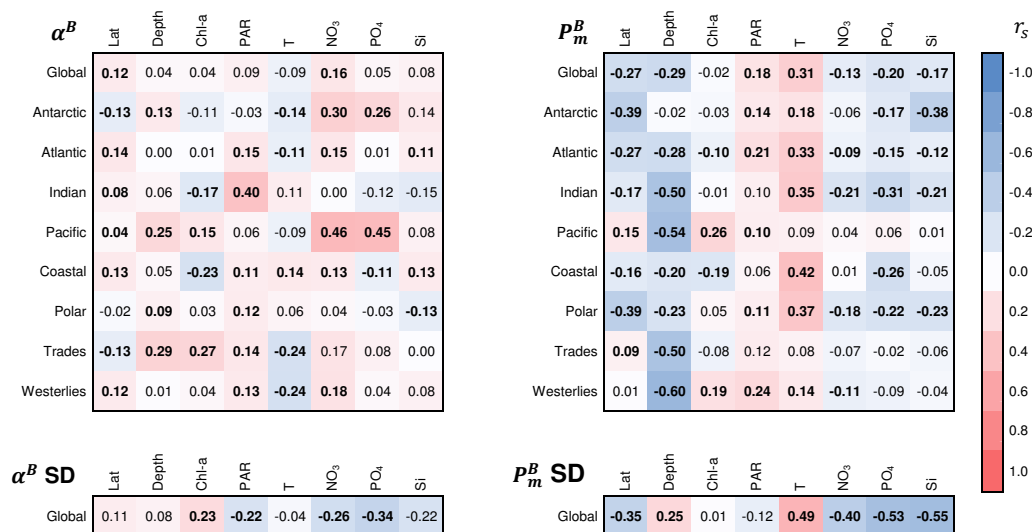
α^B

	Lat	Depth	Chl-a	PAR	T	NO$_3$	PO$_4$	Si
Global	**0.12**	0.04	0.04	0.09	-0.09	**0.16**	0.05	0.08
Antarctic	**-0.13**	**0.13**	-0.11	-0.03	**-0.14**	**0.30**	**0.26**	0.14
Atlantic	**0.14**	0.00	0.01	**0.15**	**-0.11**	**0.15**	0.01	**0.11**
Indian	**0.08**	0.06	**-0.17**	**0.40**	0.11	0.00	-0.12	-0.15
Pacific	**0.04**	**0.25**	**0.15**	0.06	-0.09	**0.46**	**0.45**	0.08
Coastal	**0.13**	0.05	**-0.23**	**0.11**	**0.14**	**0.13**	-0.11	**0.13**
Polar	-0.02	**0.09**	0.03	**0.12**	0.06	0.04	-0.03	**-0.13**
Trades	**-0.13**	**0.29**	**0.27**	**0.14**	**-0.24**	0.17	0.08	0.00
Westerlies	**0.12**	0.01	0.04	**0.13**	**-0.24**	**0.18**	0.04	0.08

P_m^B

	Lat	Depth	Chl-a	PAR	T	NO$_3$	PO$_4$	Si
Global	**-0.27**	**-0.29**	-0.02	**0.18**	**0.31**	**-0.13**	**-0.20**	**-0.17**
Antarctic	**-0.39**	-0.02	-0.03	**0.14**	**0.18**	-0.06	**-0.17**	**-0.38**
Atlantic	**-0.27**	**-0.28**	**-0.10**	**0.21**	**0.33**	**-0.09**	**-0.15**	**-0.12**
Indian	**-0.17**	**-0.50**	-0.01	0.10	**0.35**	**-0.21**	**-0.31**	**-0.21**
Pacific	**0.15**	**-0.54**	**0.26**	**0.10**	0.09	0.04	0.06	0.01
Coastal	**-0.16**	**-0.20**	**-0.19**	0.06	**0.42**	0.01	**-0.26**	-0.05
Polar	**-0.39**	**-0.23**	0.05	**0.11**	**0.37**	**-0.18**	**-0.22**	**-0.23**
Trades	**0.09**	**-0.50**	-0.08	0.12	0.08	-0.07	-0.02	-0.06
Westerlies	0.01	**-0.60**	**0.19**	**0.24**	**0.14**	**-0.11**	-0.09	-0.04

α^B SD

	Lat	Depth	Chl-a	PAR	T	NO$_3$	PO$_4$	Si
Global	0.11	0.08	**0.23**	**-0.22**	-0.04	**-0.26**	**-0.34**	**-0.22**

P_m^B SD

	Lat	Depth	Chl-a	PAR	T	NO$_3$	PO$_4$	Si
Global	**-0.35**	**0.25**	0.01	-0.12	**0.49**	**-0.40**	**-0.53**	**-0.55**

Figure 8. Spearman's Rank Correlation coefficients (r_s) for relationships between the mean and standard deviation (SD) of the initial slope (α^B) and the assimilation number (P_m^B) of the photosynthesis versus irradiance (P-I) curve and environmental variables available in the P-I database, including absolute latitude (Lat), depth, chlorophyll-*a* (Chl-a), daily photosynthetic active radiation (PAR), temperature (T), nitrate (NO$_3$), phosphate (PO$_4$) and silicate (Si). Significant relationships ($p < 0.05$) are given in bold.

4. Discussion

In the present study, a global database of photosynthesis versus irradiance (P-I) parameters, together with a 20-year time series of remote-sensing based chlorophyll-*a* concentrations, was used to study the magnitude and variability in marine primary production on a global scale. The estimate for global annual primary production of 38.8-42.1 Gt C y^{-1} between 1998 and 2018 in this study was within the range reported before (32.0-70.7 Gt C y^{-1}) [5,104] and close to earlier reported values for depth- and wavelength-resolved primary production models ($\sim$44 Gt C y^{-1}) [2,4,5,7,22]. According to the model used in this study, primary production depends on phytoplankton biomass (in chlorophyll units), photosynthetic active radiation (PAR, 400-700 nm; total value and its spectral and angular distribution) and on the assigned values of the photosynthetic and chlorophyll-*a* profile parameters. Although the model does not explicitly include the effects of environmental variables such as temperature and nutrients, or mixed-layer dynamics, these were implicitly accounted for through the photosynthetic and chlorophyll-*a* profile parameters which were assigned by season and biogeographic province [2,16]. Based on an inter-comparison of various primary production models, it has been reported that primary production generally increases at higher chlorophyll-*a* concentrations, higher PAR and shallower mixed-layer depths, whereas variability in temperature could either increase or decrease primary production [4]. In the present study, trends in global and regional annual primary production were best explained by variations in chlorophyll-*a* concentration, which in turn may vary with seasonal, inter-annual and multi-decadal variations in physico-chemical conditions of the water column [17–19]. This study confirmed that global annual primary production varied with the ENSO and AMO [17–19,26], but not all variation in global annual primary production could be explained by large scale ocean-atmospheric oscillations. The previously reported negative (linear) trend in global annual primary production [25,27,28] was not observed in the present study. Instead a more dynamic pattern of inter-annual trends in primary production was revealed at global and regional scales (also see 26,29).

The assignment of photosynthetic parameters remains one of the major challenges in the assessment of global annual primary production using numerical models based on remote-sensing observations [31–34]. In this study, we have tackled this problem by assembling a database of around ten thousand observations that covered the majority of the biogeographic provinces of Longhurst [16]. The sensitivity of primary production to variations in the photosynthetic parameters was further studied by investigating the effect on primary production of changing P-I parameters from their mean values. P-I parameters may vary 2-10 fold among different biogeographic provinces (this study; 33,86,105). This variation may reflect natural variability, but might also be affected to some extent by small differences in measurement protocols from author to author [33,86]. In the database used here, we have tried to minimise the latter source of variability, for example by correcting α^B values for the spectral quality of the light from the lamp used in the P-I experiment (also see 33). A sensitivity analysis in which P-I parameters were adjusted by $\pm$1 standard deviation revealed that the variation in photosynthetic rates may lead to a decrease or increase in the magnitude of global annual primary production by 45-47%. Global annual primary production remained within the range of earlier observations (32.0-70.7 Gt C y^{-1}) [2,4,5,22] when both P-I parameters were adjusted by +1 standard deviation (+1 SD) (56.5-61.2 Gt C y^{-1}), but adjustments by –1 standard deviation (–1 SD) resulted in considerable lower global annual primary production rates (20.4-22.2 Gt C y^{-1}). Seasonal trends in global primary production were little affected as the magnitude of change in P-I parameters was similar among seasons. The sensitivity analysis illustrated the importance of the parameters that describe the relationship between phytoplankton biomass and PAR in the calculations of primary production, but adjusting P-I parameters by $\pm$1 standard deviation would represent the lower and upper limits of change in the photosynthetic response of phytoplankton cells. It would therefore be important to better understand the variability in P-I parameters and subsequent estimates of primary production under natural variations in environmental conditions and under global climate change.

Over the past three decades, considerable efforts have been made to establish a global database of P-I parameters (2,31,33,86; this study) and to decipher their empirical relationships with

physico-chemical and optical properties to enable prediction of photosynthetic parameters on regional and global scales [38,40,41,105–108]. The observed relationships between physico-chemical conditions and P-I parameters in the present study confirmed earlier observations that temperature may be a good predictor of P_m^B, especially in coastal regions and temperate oceanic regions where temperature and associated water column stability dictates seasonal changes in the taxonomic and size structure of phytoplankton communities [40,86,109]. We note however, that the correlation coefficient between P_m^B and temperature is nowhere higher than 0.42, indicating that the importance of other factors (such as light and nutrient availability) in determining the variability in the assimilation number cannot be ruled out. The temperature dependence of P_m^B is of particular interest for assigning photosynthetic rates on regional and global scales as sea surface temperature (SST) can be obtained from remote-sensing observations on similar spatial and temporal scales as chlorophyll-*a* concentrations. Moreover, SST is a strong predictor of global climate change [24]. However, in regions with different underlying physical forcing that experience a smaller range in temperature, such as the Arabian Sea and open ocean gyres, the relationship between temperature and P_m^B is less obvious (this study; 40,41,105,107,110). In such regions, chlorophyll-*a* concentration as well as the taxonomic and size structure of the phytoplankton community may be better indicators of variability in P_m^B [38,41,86,107,108]. The initial slope of the P-I curve (α^B) seems to be more difficult to predict based on empirical relationships with physico-chemical conditions (this study, 41,86) and it has earlier been suggested that the simplest approach to estimate α^B would be to relate α^B to the assimilation number [33,110,111]. This approach may be supported by the strong dependence of I_K (P_m^B/α^B) on latitude and depth, two spatial indicators that can be seen as general proxies of water column conditions [16,33,105].

The relationship between photosynthetic parameters and temperature is of particular interest in understanding the scope of change in primary production under global climate change. Over the past decades, SST has increased by 0.5 °C and is projected to increase a further 1.5-4.0 °C under different CO_2 emission scenarios [24]. The rise in SST and subsequent changes in stratification and nutrient loading into the euphotic zone are expected to affect phytoplankton growth and primary production [23,24]. One estimate of a potential change in annual primary production arising from variations in photosynthetic parameters under global climate change can be arrived at by using SST as the main driver of change in P_m^B. Assuming a simplified linear relationship between P_m^B and temperature in the Coastal biome (where temperature dependence of P_m^B was highest; $P_m^B = 0.13 * T + 1.82$, $r^2 = 0.872$ for T < 20 °C), P_m^B might be expected to increase by 8.3% under a rise of SST of +2 °C. Based on the relationships between P_m^B and primary production estimates presented in this study (Figure 7; assuming I_K is unchanged), annual primary production in the Coastal biome could increase by +0.69 Gt C y^{-1}. Depending on the specific relationship with temperature, variations in P-I parameters and subsequent estimates of global primary production may vary on regional scales (for example +13.4% in P_m^B in the Polar biome). The actual variation in P-I parameters and primary production under global climate change would be more complex and the interplay between different physico-chemical conditions will have a major effect on the direction of change.

5. Conclusions

It is the first time that highly quality-controlled, multi-sensor, inter-sensor-bias-corrected, ocean-colour observations extending over some two decades have been combined with increased spatial and temporal coverage of *in situ* observations of the photosynthetic parameters of phytoplankton, to compute the magnitude and variability in primary production on a global scale. This has led to a more accurate assessment of global annual primary production and its trends over the past 20 years. Variability in global annual primary production could be related to inter-annual and multi-decadal oscillations, such that the present record of ocean-colour observations is not of sufficient length to detect trends associated with climate change [112]. Here, we report an inter-annual variability (standard deviation) of ±2.9% around a mean of 40.7 Gt C y^{-1} within the two decades studied. The importance of accurately assigning photosynthetic parameters in global and regional calculations of

primary production has been illustrated by a sensitivity analysis. With the recent development of a global database of *in situ* measurements of P-I parameters [33] and the subsequent enhancement of the database (this study), photosynthetic parameters could be assigned to almost all biogeographic provinces as defined by Longhurst [16]. This considerably improved the confidence with which regional primary production can be estimated, especially in those regions that were previously known to be different from others, such as the Arabian Sea and the Antarctic Ocean [110]. Yet, the need to improve P-I data coverage in large areas of the global ocean still remains (this study, Figure 1; 33,49,86). In particular, large areas of the Pacific and Indian Ocean remain poorly sampled. Methods designed to assign photosynthetic parameters based on their relationships to other variables amenable to remote-sensing [106,110], could, in the future, lead to a more dynamic assignment of these parameters. Sea surface temperature and phytoplankton community size structure (this study; 33,38,40,41,86,105,107,108) could be suitable variables for further development of such methods for different ocean basins and biomes.

Appendix A. Model of daily, water-column primary production

Appendix A.1. Phytoplankton biomass

In the model of Platt and Sathyendranath [31] and Sathyendranath *et al.* [49], ocean-colour remote-sensing products and a standard Gaussian function are used to calculate the distribution of phytoplankton biomass ($B(z)$ in mg m^{-3}) at depth. Depth profiles of chlorophyll-*a* were computed as a shifted Gaussian function:

$$B(z) = B_0 + \frac{h}{\sigma\sqrt{2\pi}} \exp{-\left(\frac{(z - z_m)^2}{2\sigma^2}\right)} \tag{A1}$$

with

$$\rho' = \left(\frac{h}{\sigma\sqrt{2\pi}}\right) / \left(\left(\frac{h}{\sigma\sqrt{2\pi}}\right) + B_0\right) \tag{A2}$$

using the background biomass (B_0 in mg m^{-3}), the total peak biomass (h in mg m^{-2}), the depth of the chlorophyll maximum (z_m in m), the standard deviation around the peak value (σ in mg m^{-3}) and the ratio of the chlorophyll peak height to the total peak biomass at z_m (ρ', dimensionless) [52].

488 Each profile parameter can vary independently, resulting in a versatile expression that can describe
489 the biomass profile in a wide variety of oceanographic regimes. Profile parameters (h, σ and ρ') were
490 obtained for 57 biogeographic provinces [16] and 4 seasons from an archived global database of 26,232
491 *in situ* chlorophyll-*a* measurements [2,101]. At each pixel, the profile parameters were scaled such that
492 the surface biomass matched the satellite chlorophyll-*a* value. Phytoplankton biomass profiles were
493 then used for calculating the underwater light field and for estimating primary production (see below).

494 *Appendix A.2. Irradiance field*

Spectrally-resolved irradiance at the sea surface was computed using a clear-sky model and expressed
as the sum of a direct sunlight component and a diffuse skylight component. The surface direct
and diffuse components were then scaled to match the daily Photosynthetic Active Radiation
(PAR, 400-700nm) products from the National Aeronautics and Space Administration (NASA)
(https://oceancolor.gsfc.nasa.gov/) and corrected for reflection and refraction at the sea surface
assuming a flat ocean. The spectrally-resolved irradiance just below the surface was then used to
construct the underwater light field ($I(z, \lambda, \theta)$ in μmol photons m^{-2} s^{-1}), as the sum of a direct (d) and
a diffuse (s) component of solar irradiance [113]:

$$I(z, \lambda, \theta) = I_d(z - \Delta z, \lambda, \theta_d)\, e^{-K_d(z,\lambda)\Delta z} + I_d(z - \Delta z, \lambda, \theta_s)\, e^{-K_s(z,\lambda)\Delta z} \tag{A3}$$

with

$$K_d(z, \lambda) = [a(z, \lambda) + b_b(z, \lambda)]\, (\cos \theta_d)^{-1} \tag{A4}$$

$$K_s(z, \lambda) = [a(z, \lambda) + b_b(z, \lambda)]\, \langle \cos \theta_s \rangle^{-1} \tag{A5}$$

where z is the depth (in m), λ is the wavelength (in nm), θ_d is the zenith angle of sun in water (in
degrees), K_d is the light attenuation coefficient (in m^{-1}) for direct sunlight, K_s is the light attenuation
coefficient (in m^{-1}) for diffuse skylight, $a(z, \lambda)$ is the volume absorption coefficient (in m^{-1}), $b_b(z, \lambda)$
is the backscattering coefficient (in m^{-1}) and $\langle \cos \theta_s \rangle$ is the mean cosine for the angular distribution
of diffuse skylight after refraction at the sea surface [31,102]. The calculations make use of the
chlorophyll-*a* profile to account for the influence of depth-dependent biomass on the light attenuation
coefficient at each depth. The value of $a(z, \lambda)$ is expressed as the sum of the contributions to absorption
from pure seawater, phytoplankton, coloured dissolved organic matter and detritus. Absorption by
phytoplankton depends on the concentration of chlorophyll-*a* ($B(z)$):

$$a_B(z, \lambda) = a_B^*(\lambda)\, B(z) \tag{A6}$$

where $a_B^*(\lambda)$ is the chlorophyll-*a* specific absorption coefficient (in m^2 mg Chl-a^{-1}) at wavelength
λ. Concentrations of $B(z)$ were obtained from ocean-colour remote-sensing observations (see main
text) and expressed as the sum of chlorophyll-*a* concentrations contained in three size classes: pico-
(p), nano- (n) and microphytoplankton (m). Phytoplankton absorption $a_B(z, \lambda)$ was estimated as the
sum of the contributions of pico-, nano- and microphytoplankon to total phytoplankton absorption
following Brewin *et al.* [96,97]:

$$\begin{aligned}
a_B(z, \lambda) = \;& a_p^*(\lambda)\, B_p^m\, [1 - \exp(-S_p\, B(z))] \\
& + a_n^*(\lambda)\, \{B_{p,n}^m\, [1 - \exp(-S_{p,n}\, B(z))] - B_p^m\, [1 - \exp(-S_p\, B(z))]\} \\
& + a_m^*(\lambda)\, \{B(z) - B_{p,n}^m\, [1 - \exp(-S_{p,n}\, B(z))]\}\,.
\end{aligned} \tag{A7}$$

495 Here, the size-specific absorption coefficients $a_p^*(\lambda)$, $a_n^*(\lambda)$ and $a_m^*(\lambda)$ (in m^2 mg Chl-a^{-1}) are the
496 values reported by Brewin *et al.* [96] and the fitted parameters B_p^m (0.13 mg Chl-a m^{-3}) and $B_{p,n}^m$ (0.77
497 mg Chl-a m^{-3}) are the maximum concentrations attainable by picophytoplankton and combined
498 pico- and nanophytoplankton, respectively. The parameters S_p (6.15 m^3 mg Chl-a^{-1}) and $S_{p,n}$ (1.26

m^3 mg Chl-a^{-1}) determine the rate of change in the chlorophyll-*a* concentrations associated with picophytoplankton and the combined concentration of pico- and nanophytoplankton with changes in total chlorophyll-*a* concentration (model parameters are from Brewin *et al.* [97]).

Similar to absorption, the total backscattering coefficient b_b used in equations (A4) and (A5) depends on back-scattering by pure seawater and by chlorophyll-*a* concentration, as in Sathyendranath *et al.* [114]:

$$b_b(z, \lambda) = b_{bw}(\lambda) + b_{bB}(z, \lambda) \tag{A8}$$

with $b_{bw}(z, \lambda)$ being the backscattering coefficient of water according to Morel [115] and $b_{bB}(z)$ the particle backscattering coefficient modelled as a function of chlorophyll-*a* concentration as in Sathyendranath *et al.* [114], following [116] and Loisel and Morel [117].

Appendix A.3. Daily primary production over the water column

The model of Platt and Sathyendranath [31], with the updates as in Sathyendranath *et al.* [49], uses a local algorithm based on surface biomass fields from ocean-colour remote-sensing, chlorophyll-*a* profile parameters, irradiance resolved with wavelength, angular distribution and depth, and photosynthesis versus irradiance (P-I) parameters to estimate water column primary production. Here, by the word "local" we imply that the model is implemented with parameters that are specific to the location and time. Primary production at depth z and time t ($P^B(z, t)$ in mg C mg Chl-a^{-1} h^{-1}) is given by:

$$P^B(z, t) = P_m^B(z, t) \left(1 - \exp\left[\frac{-\Pi^B(z, t)}{P_m^B(z, t)} \right] \right) \tag{A9}$$

where

$$\Pi^B(z, t) = \int_{400}^{700} \alpha^B(z, t, \lambda) \left[I_d(z, t, \lambda, \theta_d) \sec \theta_d + 1.20 \, I_s(z, t, \lambda) \right] d\lambda \tag{A10}$$

where $\alpha^B(z, t, \lambda)$ is the photosynthetic action spectrum (in mg C mg Chl-a^{-1} h^{-1} (μmol photons m^{-2} s^{-1})$^{-1}$) and integrals are taken over the range of PAR (400-700 nm) [31,37]. In equation (A10), the shape of $\alpha^B(z, t, \lambda)$ is scaled such that the mean value is equal to the non-spectral value of α^B for flat, white light [118] and the spectral shape of α^B is taken to be the same as that of the phytoplankton absorption spectrum. Note that the P-I parameters do not change with depth in the present primary production model.

Model calculations were performed at 9 km spatial resolution using a wavelength resolution of 5 nm, a depth interval of 0.5 m from the surface to the euphotic depth (depth at which light is reduced to 1% of its value at the surface) and at 12 time steps from dawn till local noon. The computed production at each depth and at at each time step was summed over depth and time, and then multiplied by two to obtain daily, water column primary production. In the event of any missing data in monthly OC-CCI chlorophyll-*a* fields, the computed primary production in each biogeographic province and in each month was scaled to full coverage using the mean primary production and the area of that province, with a weighting function accounting for variability in PAR in the specific biogeographic province. Mean monthly production (in mg C m^{-2} d^{-1}) in each biogeographic province was then summed to obtain global annual primary production (in Gt C y^{-1}) for each year between 1998 and 2018.

523 ## Appendix B. Biogeographic provinces

Table A1. List of biogeographic provinces according to Longhurst (2007).

Number	Basin	Biome	Acronym	Province
1	Atlantic	Polar	BPLR	Boreal Polar Province
2	Atlantic	Polar	ARCT	Atlantic Arctic Province
3	Atlantic	Polar	SARC	Atlantic Subarctic Province
4	Atlantic	Westerlies	NADR	North Atlantic Drift Province
5	Atlantic	Westerlies	GFST	Gulf Stream Province
6	Atlantic	Westerlies	NASW	North Atlantic Subtropical Gyral Province (West)
7	Atlantic	Trades	NATR	North Atlantic Tropical Gyral Province
8	Atlantic	Trades	WTRA	Western Tropical Atlantic Province
9	Atlantic	Trades	ETRA	Eastern Tropical Atlantic Province
10	Atlantic	Trades	SATL	South Atlantic Gyral Province
11	Atlantic	Coastal	NECS	Northeast Atlantic Shelves Province
12	Atlantic	Coastal	CNRY	Canary Current Coastal Province
13	Atlantic	Coastal	GUIN	Guinea Current Coastal Province
14	Atlantic	Coastal	GUIA	Guianas Coastal Province
15	Atlantic	Coastal	NWCS	Northwest Atlantic Shelves Province
16	Atlantic	Westerlies	MEDI	Mediterranean Sea, Black Sea Province
17	Atlantic	Trades	CARB	Caribbean Province
18	Atlantic	Westerlies	NASE	North Atlantic Subtropical Gyral Province (East)
19	Atlantic	Coastal	CHSB	Cheasapeake Bay Province
20	Atlantic	Coastal	BRAZ	Brazil Current Coastal Province
21	Atlantic	Coastal	FKLD	Southwest Atlantic Shelves Province
22	Atlantic	Coastal	BENG	Benguela Current Coastal Province
30	Indian	Trades	MONS	Indian Monsoon Gyres Province
31	Indian	Trades	ISSG	Indian South Subtropical Gyre Province
32	Indian	Coastal	EAFR	Eastern Africa Coastal Province
33	Indian	Coastal	REDS	Red Sea, Arabian Gulf Province
34	Indian	Coastal	ARAB	Northwest Arabian Sea Upwelling Province
35	Indian	Coastal	INDE	Eastern India Coastal Province
36	Indian	Coastal	INDW	Western India Coastal Province
37	Indian	Coastal	AUSW	Australia-Indonesia Coastal Province
50	Pacific	Polar	BERS	North Epicontinental Sea Province
51	Pacific	Westerlies	PSAE	Pacific Subarctic Gyres Province (East)
52	Pacific	Westerlies	PSAW	Pacific Subarctic Gyres Province (West)
53	Pacific	Westerlies	KURO	Kuroshio Current Province
54	Pacific	Westerlies	NPPF	North Pacific Polar Front Province
55	Pacific	Westerlies	NPSE	North Pacific Subtropical Province (East)
56	Pacific	Westerlies	NPSW	North Pacific Subtropical Province (West)
57	Pacific	Westerlies	OCAL	Offshore California Current Province
58	Pacific	Westerlies	TASM	Tasman Sea Province
59	Pacific	Westerlies	SPSG	South Pacific Subtropical Gyre Province
60	Pacific	Trades	NPTG	North Pacific Tropical Gyre Province
61	Pacific	Trades	PNEC	North Pacific Equatorial Countercurrent Province
62	Pacific	Trades	PEQD	Pacific Equatorial Divergence Province
63	Pacific	Trades	WARM	Western Pacific Warm Pool Province
64	Pacific	Trades	ARCH	Archipelagic Deep Basin Province
65	Pacific	Coastal	ALSK	Alaska Coastal Downwelling Province
66	Pacific	Coastal	CCAL	California Upwelling Coastal Province
67	Pacific	Coastal	CAMR	Central American Coastal Province
68	Pacific	Coastal	CHIL	Chile–Peru Current Coastal Province
69	Pacific	Coastal	CHIN	China Sea Coastal Province
70	Pacific	Coastal	SUND	Sunda-Arafura Shelves Province
71	Pacific	Coastal	AUSE	Eastern Australian Coastal Province
72	Pacific	Coastal	NEWZ	New Zealand Coastal Province
80	Antarctic	Westerlies	SSTC	South Subtropical Convergence Province
81	Antarctic	Westerlies	SANT	Subantarctic Water Ring Province
82	Antarctic	Polar	ANTA	Antarctic Province
83	Antarctic	Polar	APLR	Austral Polar Province

References

1. Lurin, B.; Rasool, S.; Cramer.W..; Moore.B.. Global terrestrial net primary production. *Global Change Newsletter (IGBP)* **1994**, *19*, 6–8.

2. Longhurst, A.R.; Sathyendranath, S.; Platt, T.; Caverhill, C. An estimate of global primary production in the ocean from satellite radiometer data. *Journal of Plankton Research* **1995**, *17*, 1245–1271. doi:10.1093/plankt/17.6.1245.

3. Field, C.B. Primary Production of the Biosphere: Integrating Terrestrial and Oceanic Components. *Science* **1998**, *281*, 237–240. doi:10.1126/science.281.5374.237.

4. Carr, M.E.; Friedrichs, M.A.; Schmeltz, M.; Noguchi Aita, M.; Antoine, D.; Arrigo, K.R.; Asanuma, I.; Aumont, O.; Barber, R.; Behrenfeld, M.; Bidigare, R.; Buitenhuis, E.T.; Campbell, J.; Ciotti, A.; Dierssen, H.; Dowell, M.; Dunne, J.; Esaias, W.; Gentili, B.; Gregg, W.; Groom, S.; Hoepffner, N.; Ishizaka, J.; Kameda, T.; Le Quéré, C.; Lohrenz, S.; Marra, J.; Mélin, F.; Moore, K.; Morel, A.; Reddy, T.E.; Ryan, J.; Scardi, M.; Smyth, T.; Turpie, K.; Tilstone, G.; Waters, K.; Yamanaka, Y. A comparison of global estimates of marine primary production from ocean color. *Deep-Sea Research Part II: Topical Studies in Oceanography* **2006**, *53*, 741–770. doi:10.1016/j.dsr2.2006.01.028.

5. Buitenhuis, E.T.; Hashioka, T.; Quéré, C.L. Combined constraints on global ocean primary production using observations and models. *Global Biogeochemical Cycles* **2013**, *27*, 847–858. doi:10.1002/gbc.20074.

6. Falkowski, P.G.; Barber, R.T.; Smetacek, V. Biogeochemical controls and feedbacks on ocean primary production. *Science* **1998**, *281*, 200–206. doi:10.1126/science.281.5374.200.

7. Antoine, D.; André, J.M.; Morel, A. Oceanic primary production 2. Estimation at global scale from satellite (coastal zone color scanner) chlorophyll. *Global Biogeochemical Cycles* **1996**, *10*, 57–69.

8. von Schuckmann, K.; Le Traon, P.Y.; Alvarez-Fanjul, E.; Axell, L.; Balmaseda, M.; Breivik, L.A.; Brewin, R.J.; Bricaud, C.; Drevillon, M.; Drillet, Y.; Dubois, C.; Embury, O.; Etienne, H.; Sotillo, M.G.; Garric, G.; Gasparin, F.; Gutknecht, E.; Guinehut, S.; Hernandez, F.; Juza, M.; Karlson, B.; Korres, G.; Legeais, J.F.; Levier, B.; Lien, V.S.; Morrow, R.; Notarstefano, G.; Parent, L.; Pascual, Á.; Pérez-Gómez, B.; Perruche, C.; Pinardi, N.; Pisano, A.; Poulain, P.M.; Pujol, I.M.; Raj, R.P.; Raudsepp, U.; Roquet, H.; Samuelsen, A.; Sathyendranath, S.; She, J.; Simoncelli, S.; Solidoro, C.; Tinker, J.; Tintoré, J.; Viktorsson, L.; Ablain, M.; Almroth-Rosell, E.; Bonaduce, A.; Clementi, E.; Cossarini, G.; Dagneaux, Q.; Desportes, C.; Dye, S.; Fratianni, C.; Good, S.; Greiner, E.; Gourrion, J.; Hamon, M.; Holt, J.; Hyder, P.; Kennedy, J.; Manzano-Muñoz, F.; Melet, A.; Meyssignac, B.; Mulet, S.; Buongiorno Nardelli, B.; O'Dea, E.; Olason, E.; Paulmier, A.; Pérez-González, I.; Reid, R.; Racault, M.F.; Raitsos, D.E.; Ramos, A.; Sykes, P.; Szekely, T.; Verbrugge, N. The Copernicus Marine Environment Monitoring Service Ocean State Report. *Journal of Operational Oceanography* **2016**, *9*, s235–s320. doi:10.1080/1755876X.2016.1273446.

9. Le Quéré, C.; Andrew, R.; Friedlingstein, P.; Sitch, S.; Hauck, J.; Pongratz, J.; Pickers, P.; Ivar Korsbakken, J.; Peters, G.; Canadell, J.; Arneth, A.; Arora, V.; Barbero, L.; Bastos, A.; Bopp, L.; Ciais, P.; Chini, L.; Ciais, P.; Doney, S.; Gkritzalis, T.; Goll, D.; Harris, I.; Haverd, V.; Hoffman, F.; Hoppema, M.; Houghton, R.; Hurtt, G.; Ilyina, T.; Jain, A.; Johannessen, T.; Jones, C.; Kato, E.; Keeling, R.; Klein Goldewijk, K.; Landschützer, P.; Lefèvre, N.; Lienert, S.; Liu, Z.; Lombardozzi, D.; Metzl, N.; Munro, D.; Nabel, J.; Nakaoka, S.I.; Neill, C.; Olsen, A.; Ono, T.; Patra, P.; Peregon, A.; Peters, W.; Peylin, P.; Pfeil, B.; Pierrot, D.; Poulter, B.; Rehder, G.; Resplandy, L.; Robertson, E.; Rocher, M.; Rödenbeck, C.; Schuster, U.; Skjelvan, I.; Séférian, R.; Skjelvan, I.; Steinhoff, T.; Sutton, A.; Tans, P.; Tian, H.; Tilbrook, B.; Tubiello, F.; Van Der Laan-Luijkx, I.; Van Der Werf, G.; Viovy, N.; Walker, A.; Wiltshire, A.; Wright, R.; Zaehle, S.; Zheng, B. Global Carbon Budget 2018. *Earth System Science Data* **2018**, *10*, 2141–2194. doi:10.5194/essd-10-2141-2018.

10. Sathyendranath, S.; Brewin, R.J.W.; Brockmann, C.; Brotas, V.; Calton, B.; Chuprin, A.; Cipollini, P.; Couto, A.B.; Dingle, J.; Doerffer, R.; Donlon, C.; Dowell, M.; Farman, A.; Grant, M.; Groom, S.; Horseman, A.; Jackson, T.; Krasemann, H.; Lavender, S.; Martinez-Vicente, V.; Mazeran, C.; Mélin, F.; Moore, T.S.; Müller, D.; Regner, P.; Roy, S.; Steele, C.J.; Steinmetz, F.; Swinton, J.; Taberner, M.; Thompson, A.; Valente, A.; Zühlke, M.; Brando, V.E.; Feng, H.; Feldman, G.; Franz, B.A.; Frouin, R.; Gould, Jr., R.W.; Hooker, S.B.; Kahru, M.; Kratzer, S.; Mitchell, B.G.; Muller-Karger, F.; Sosik, H.M.; Voss, K.J.; Werdell, J.; Platt, T. An ocean-colour time series for use in climate studies: the experience of the Ocean-Colour Climate Change Initiative (OC-CCI). *Sensors* **2019**, *19*, 4285. doi:doi:10.3390/s19194285.

11. Montes-Hugo, M.; Doney, S.C.; Ducklow, H.W.; Fraser, W.; Martinson, D.; Stammerjohn, S.E.; Schofield, O. Recent changes in phytoplankton communities associated with rapid regional climate change along the western Antarctic Peninsula. *Science* **2009**, *323*, 1470–1473. doi:10.1126/science.1164533.

12. Arrigo, K.R.; Van Dijken, G.L. Continued increases in Arctic Ocean primary production. *Progress in Oceanography* **2015**, *136*, 60–70. doi:10.1016/j.pocean.2015.05.002.

13. Randelhoff, A.; Oziel, L.; Massicotte, P.; Bécu, G.; Galí, M.; Lacour, L.; Dumont, D.; Vladoiu, A.; Marec, C.; Bruyant, F.; Houssais, M.N.; Tremblay, J..; Deslongchamps, G.; Babin, M. The evolution of light and vertical mixing across a phytoplankton ice-edge bloom. *Elementa Science of the Anthropocene* **2019**, *7*, 20. doi:10.1525/elementa.357.

14. Oziel, L.; Massicotte, P.; Randelhoff, A.; Ferland, J.; Vladoiu, A.; Lacour, L.; Galindo, V.; Lambert-Girard, S.; Dumont, D.; Cuypers, Y.; Bouruet-Aubertot, P.; Mundy, C.J.; Ehn, J.; Bécu, G.; Marec, C.; Forget, M.H.; Garcia, N.; Coupel, P.; Raimbault, P.; Houssais, M.N.; Babin, M. Environmental factors influencing the seasonal dynamics of spring algal blooms in and beneath sea ice in western Baffin Bay. *Elementa Science of the Anthropocene* **2019**, *7*, 34. doi:10.1525/elementa.372.

15. Karl, D.M.; Christian, J.R.; Dore, J.E.; Hebel, D.V.; Letelier, R.M.; Tupas, L.M.; Winn, C.D. Seasonal and interannual variability in primary production and particle flux at station ALOHA. *Deep-Sea Research Part II: Topical Studies in Oceanography* **1996**, *43*, 539–568.

16. Longhurst, A.R. *Ecological geography of the sea*, 2nd ed.; Elsevier Academic Press, 2007; p. 542.

17. Di Lorenzo, E.; Schneider, N.; Cobb, K.M.; Franks, P.J.; Chhak, K.; Miller, A.J.; McWilliams, J.C.; Bograd, S.J.; Arango, H.; Curchitser, E.; Powell, T.M.; Rivière, P. North Pacific Gyre Oscillation links ocean climate and ecosystem change. *Geophysical Research Letters* **2008**, *35*, 2–7. doi:10.1029/2007GL032838.

18. Martinez, E.; Antoine, D.; D'Ortenzio, F.; Gentili, B. Climate-driven basin-scale decadal oscillations of oceanic phytoplankton. *Science* **2009**, *326*, 1253–1256. doi:10.1126/science.1177012.

19. Racault, M.F.; Sathyendranath, S.; Brewin, R.J.; Raitsos, D.E.; Jackson, T.; Platt, T. Impact of El Niño variability on oceanic phytoplankton. *Frontiers in Marine Science* **2017**, *4*, 133. doi:10.3389/fmars.2017.00133.

20. Lan, K.W.; Evans, K.; Lee, M.A. Effects of climate variability on the distribution and fishing conditions of yellowfin tuna (Thunnus albacares) in the western Indian Ocean. *Climatic Change* **2013**, *119*, 63–77. doi:10.1007/s10584-012-0637-8.

21. Taboada, F.G.; Barton, A.D.; Stock, C.A.; Dunne, J.; John, J.G. Seasonal to interannual predictability of oceanic net primary production inferred from satellite observations. *Progress in Oceanography* **2019**, *170*, 28–39. doi:10.1016/j.pocean.2018.10.010.

22. Westberry, T.; Behrenfeld, M.J.; Siegel, D.A.; Boss, E. Carbon-based primary productivity modeling with vertically resolved photoacclimation. *Global Biogeochemical Cycles* **2008**, *22*, 1–18. doi:10.1029/2007GB003078.

23. Field, C.; Barros, V.; Dokken, D.; Mach, K.; Mastrandrea, M.; Bilir, T.; Chatterjee, M.; Ebi, K.; Estrada, Y.; Genova, R.; Girma, B.; Kissel, E.; Levy, A.; MacCracken, S.; Mastrandrea, P.; White, L. *IPCC, 2014: Climate Change 2014: Impacts, Adaptation, and Vulnerability. Part A: Global and Sectoral Aspects. Contribution of Working Group II to the Fifth Assessment Report of the Intergovernmental Panel on Climate Change*; Cambridge University Press, Cambridge, United Kingdom and New York, NY, USA, 2014; p. 1132.

24. Rhein, M.; Rintoul, S.; Aoki, S.; Campos, E.; Chambers, D.; Feely, R.; Gulev, S.; Johnson, G.; Josey, S.; Kostianoy, A.; Mauritzen, C.; Roemmich, D.; Talley, L.; Wang, F. Observations: Ocean. In *Climate Change 2013: The Physical Science Basis. Contribution of Working Group I to the Fifth Assessment Report of the Intergovernmental Panel on Climate Change*; Stocker, T.; Qin, D.; Plattner, G.K.; Tignor, M.; Allen, S.; Boschung, J.; Nauels, A.; Xia, Y.; Bex, V.; Midgley, P., Eds.; Cambridge University Press, Cambridge, United Kingdom and New York, NY, USA, 2013; pp. 255–316.

25. Behrenfeld, M.J.; O'Malley, R.T.; Siegel, D.a.; McClain, C.R.; Sarmiento, J.L.; Feldman, G.C.; Milligan, A.J.; Falkowski, P.G.; Letelier, R.M.; Boss, E.S. Climate-driven trends in contemporary ocean productivity. *Nature* **2006**, *444*, 752–755. doi:10.1038/nature05317.

26. Chavez, F.P.; Messié, M.; Pennington, J.T. Marine Primary Production in Relation to Climate Variability and Change. *Annual Review of Marine Science* **2011**, *3*, 227–260. doi:10.1146/annurev.marine.010908.163917.

27. Polovina, J.J.; Dunne, J.P.; Woodworth, P.A.; Howell, E.A. Projected expansion of the subtropical biome and contraction of the temperate and equatorial upwelling biomes in the North Pacific under global warming. *ICES Journal of Marine Science* **2011**, *68*, 986–995. doi:10.1093/icesjms/fsq198.

28. Gregg, W.; Rousseaux, C.S. Global ocean primary production trends in the modern ocean color satellite record (1998-2015). *Environmental Research Letters* **2019**, *14*, 124011. doi:10.1088/1748-9326/ab4667.

29. Saba, V.S.; Friedrichs, M.A.; Carr, M.E.; Antoine, D.; Armstrong, R.A.; Asanuma, I.; Aumont, O.; Bates, N.R.; Behrenfeld, M.J.; Bennington, V.; Bopp, L.; Bruggeman, J.; Buitenhuis, E.T.; Church, M.J.; Ciotti, A.M.; Doney, S.C.; Dowell, M.; Dunne, J.; Dutkiewicz, S.; Gregg, W.; Hoepffner, N.; Hyde, K.J.; Ishizaka, J.; Kameda, T.; Karl, D.M.; Lima, I.; Lomas, M.W.; Marra, J.; McKinley, G.A.; Melin, F.; Moore, J.K.; Morel, A.; O'Reilly, J.; Salihoglu, B.; Scardi, M.; Smyth, T.J.; Tang, S.; Tjiputra, J.; Uitz, J.; Vichi, M.; Waters, K.; Westberry, T.K.; Yool, A. Challenges of modeling depth-integrated marine primary productivity over multiple decades: A case study at BATS and HOT. *Global Biogeochemical Cycles* **2010**, *24*, 1–21. doi:10.1029/2009GB003655.

30. Pörtner, H.O.; Karl, D.; Boyd, P.; Cheung, W.; Lluch-Cota, S.; Nojiri, Y.; Schmidt, D.; Zavialov, P. Ocean systems. In *Climate Change 2014: Impacts, Adaptation, and Vulnerability. Part A: Global and Sectoral Aspects. Contribution of Working Group II to the Fifth Assessment Report of the Intergovernmental Panel on Climate Change*; Field, C.; Barros, V.; Dokken, D.; Mach, K.; Mastrandrea, M.; Bilir, T.; Chatterjee, M.; Ebi, K.; Estrada, Y.; Genova, R.; Girma, B.; Kissel, E.; Levy, A.; MacCracken, S.; Mastrandrea, P.; White, L., Eds.; Cambridge University Press, Cambridge, United Kingdom and New York, NY, USA, 2014; pp. 411–484.

31. Platt, T.; Sathyendranath, S. Oceanic primary production: Estimation by remote sensing at local and regional scales. *Science* **1988**, *241*, 1613–1620. doi:10.1126/science.241.4873.1613.

32. Platt, T.; Sathyendranath, S. Spatial structure of pelagic ecosystem processes in the global ocean. *Ecosystems* **1999**, *2*, 384–394.

33. Bouman, H.A.; Platt, T.; Doblin, M.; Figueiras, F.G.; Gudmundsson, K.; Gudfinnsson, H.G.; Huang, B.; Hickman, A.; Hiscock, M.; Jackson, T.; Lutz, V.A.; Mélin, F.; Rey, F.; Pepin, P.; Segura, V.; Tilstone, G.H.; van Dongen-Vogels, V.; Sathyendranath, S. Photosynthesis-irradiance parameters of marine phytoplankton: Synthesis of a global data set. *Earth System Science Data* **2018**, *10*, 251–266. doi:10.5194/essd-10-251-2018.

34. Sathyendranath, S.; Platt, T. Remote sensing of water-column primary production. In *Measurement of Primary Production from the Molecular to the Global Scale*; Li, W.K.W.; Maestrini, S.Y., Eds.; ICES Marine Science Symposia: Copenhagen, 1993; Vol. 197, pp. 236–243.

35. Friedrichs, M.A.; Carr, M.E.; Barber, R.T.; Scardi, M.; Antoine, D.; Armstrong, R.A.; Asanuma, I.; Behrenfeld, M.J.; Buitenhuis, E.T.; Chai, F.; Christian, J.R.; Ciotti, A.M.; Doney, S.C.; Dowell, M.; Dunne, J.; Gentili, B.; Gregg, W.; Hoepffner, N.; Ishizaka, J.; Kameda, T.; Lima, I.; Marra, J.; Mélin, F.; Moore, J.K.; Morel, A.; O'Malley, R.T.; O'Reilly, J.; Saba, V.S.; Schmeltz, M.; Smyth, T.J.; Tjiputra, J.; Waters, K.; Westberry, T.K.; Winguth, A. Assessing the uncertainties of model estimates of primary productivity in the tropical Pacific Ocean. *Journal of Marine Systems* **2009**, *76*, 113–133. doi:10.1016/j.jmarsys.2008.05.010.

36. Jassby, A.D.; Platt, T. Mathematical formulation of the relationship between photosynthesis and light for phytoplankton. *Limnology and Oceanography* **1976**, *21*, 540–547. doi:10.4319/lo.1976.21.4.0540.

37. Platt, T.; Gallegos, C.L.; Harrison, W.G. Photoinhibition of photosynthesis in natural assemblages of marine phytoplankton. *Journal of Marine Research* **1980**, *38*, 103–111.

38. Côté, B.; Platt, T. Day-to-day variations in the spring-summer photosynthetic parameters of coastal marine phytoplankton. *Limnology and Oceanography* **1983**, *28*, 320–344. doi:10.4319/lo.1983.28.2.0320.

39. Platt, T.; Sathyendranath, S.; Ulloa, O.; Harrison, W.G.; Hoepffner, N.; Goes, J. Nutrient control of phytoplankton photosynthesis in the Western North Atlantic. *Nature* **1992**, *356*, 229–231.

40. Bouman, H.; Platt, T.; Sathyendranath, S.; Stuart, V. Dependence of light-saturated photosynthesis on temperature and community structure. *Deep-Sea Research Part I: Oceanographic Research Papers* **2005**, *52*, 1284–1299. doi:10.1016/j.dsr.2005.01.008.

41. Huot, Y.; Babin, M.; Bruyant, F.; Grob, C.; Twardowski, M.S.; Claustre, H. Relationship between photosynthetic parameters and different proxies of phytoplankton biomass in the subtropical ocean. *Biogeosciences* **2007**, *4*, 853–868. doi:10.5194/bg-4-853-2007.

42. Uitz, J.; Huot, Y.; Bruyant, F.; Babin, M.; Claustre, H. Relating phytoplankton photophysiological properties to community structure on large scale. *Limnology and Oceanography* **2008**, *53*, 614–630.

43. Uitz, J.; Claustre, H.; Gentili, B.; Stramski, D. Phytoplankton class-specific primary production in the world's oceans: Seasonal and interannual variability from satellite observations. *Global Biogeochemical Cycles* **2010**, *24*, GB3016. doi:10.1029/2009GB003680.

44. Mélin, F. Potentiel de la télédétection pour l'analyse des propriétés optiques du système océan-atmosphère et application à l'estimation de la photosynthèse phytoplanctonique. PhD thesis, Université Toulouse III, Toulouse, France, 1993.

45. Mélin, F.; Hoepffner, N. Global marine primary production: a satellite view. Technical report, Institute for Environment and Sustainability, Ispra, Varese, Italy, 2004.

46. Platt, T.; Sathyendranath, S. Estimators of primary production for interpretation of remotely sensed data on ocean color. *Journal of Geophysical Research* **1993**, *98*, 14,561–14,576.

47. Sathyendranath, S.; Platt, T. Spectral effects in bio-optical control on the ocean system. *Oceanologia* **2007**, *49*, 5–39.

48. Sathyendranath, S.; Stuart, V.; Nair, A.; Oka, K.; Nakane, T.; Bouman, H.; Forget, M.H.; Maass, H.; Platt, T. Carbon-to-chlorophyll ratio and growth rate of phytoplankton in the sea. *Marine Ecology Progress Series* **2009**, *383*, 73–84. doi:10.3354/meps07998.

49. Sathyendranath, S.; Platt, T.; Žarko Kovač.; Dingle, J.; Jackson, T.; Brewin, R.J.W.; Franks, P.; nón, E.M.; Kulk, G.; Bouman, H. Reconciling models of primary production and photoacclimation. *Applied Optics* **2020**, p. Submitted.

50. Platt, T.; Sathyendranath, S. Biological production models as elements of coupled, atmosphere-ocean models for climate research. *Journal of Geophysical Research* **1991**, *96*, 2585–2592.

51. Kyewalyanga, M.; Platt, T.; Sathyendranath, S. Ocean primary production calculated by spectral and broad-band models. *Marine Ecology Progress Series* **1992**, *85*, 171–185.

52. Sathyendranath, S.; Longhurst, A.; Caverhill, C.M.; Platt, T. Regionally and seasonally differentiated primary production in the North Atlantic. *Deep-Sea Research I* **1995**, *42*, 1773–1802.

53. Lobanova, P.; Tilstone, G.H.; Bashmachnikov, I.; Brotas, V. Accuracy assessment of primary production models with and without photoinhibition using Ocean-Colour climate change initiative data in the North East Atlantic Ocean. *Remote Sensing* **2018**, *10*, 1–24. doi:10.3390/rs10071116.

54. Sathyendranath, S.; Jackson, T.; Brockmann, C.; Brotas, V.; Calton, B.; Chuprin, A.; Clements, O.; Cipollini, P.; Danne, O.; Dingle, J.; et al.. ESA Ocean Colour Climate Change Initiative (Ocean_Colour_cci): Version 4.0 Data. Technical report, Centre for Environmental Data Analysis: Harwell,UK, 2019. doi:http://catalogue.ceda.ac.uk/uuid/00b5fc99f9384782976a4453b0148f49.

55. Mélin, F.; Vantrepotte, V.; Chuprin, A.; Grant, M.; Jackson, T.; S., S. Assessing the fitness-for-purpose of satellite multi-mission ocean color climate data records: A protocol applied to OC-CCI chlorophyll-a data. *Remote Sensing of Environment* **2017**, *203*, 139–151. doi:10.1016/j.rse.2017.03.039.

56. Bouman, H.A.; Platt, T.; Doblin, M.A.; Figueiras, F.G.; Gudmundsson, K.; Gudfinnsson, H.G.; Huang, B.; Hickman, A.; Hiscock, M.R.; Jackson, T.; Lutz, V.A.; Mélin, F.; Rey, F.; Pepin, P.; Segura, V.; Tilstone, G.; van Dongen-Vogels, V.; Sathyendranath, S. A global dataset of photosynthesis-irradiance parameters for marine phytoplankton. *PANGAEA* **2017**, *874087*. doi:doi.org/10.1594/PANGAEA.874087.

57. Thomas, W.H. On nitrogen deficiency in tropical Pacific oceanic phytoplankton: Photosynthetic parameters in poor and rich water. *Limnology and Oceanography* **1970**, *15*, 380–385.

58. Hameedi, M.J. Changes in specific photosynthetic rate of oceanic phytoplankton from the northeast Pacific Ocean. *Helgoländer Wissenschaftliche Meeresuntersuchungen* **1977**, *30*, 62–75. doi:10.1007/BF02207825.

59. Cole, B.; Cloern, J. Significance of biomass and light availability to phytoplankton productivity in San Francisco Bay. *Marine Ecology Progress Series* **1984**, *17*, 15–24. doi:10.3354/meps017015.

60. Harding, L.; Meeson, B.; Fisher, T. Photosynthesis patterns in Chesapeake Bay phytoplankton: short- and long-term responses of P-l curve parameters to light. *Marine Ecology Progress Series* **1985**, *26*, 99–111. doi:10.3354/meps026099.

61. Harding, L.W.; Meeson, B.W.; Fisher, T.R. Phytoplankton production in two east coast estuaries: Photosynthesis-light functions and patterns of carbon assimilation in Chesapeake and Delaware Bays. *Estuarine, Coastal and Shelf Science* **1986**, *23*, 773–806. doi:10.1016/0272-7714(86)90074-0.

62. Forbes, J.; Denman, K.; Mackas, D. Determination of photosynthetic capacity in coastal marine phytoplankton: effects of assay irradiance and variability of photosynthetic parameters. *Marine Ecology Progress Series* **1986**, *32*, 181–191. doi:10.3354/meps032181.

63. Welschmeyer, N.; Goericke, R.; Strom, S.; Peterson, W. Phytoplankton growth and herbivory in the subarctic Pacific: A chemotaxonomic analysis. *Limnology and Oceanography* **1991**, *36*, 1631–1649. doi:10.4319/lo.1991.36.8.1631.

64. Gallegos, C.L. Phytoplankton photosynthesis, productivity, and species composition in a eutrophic eastuary: Comparison of bloom and non-bloom assemblages. *Marine Ecology Progress Series* **1992**, *81*, 257–267.

65. Vant, W.N.; Budd, R.G. Phytoplankton photosynthesis and growth in contrasting regions of Manukau harbour, New Zealand. *New Zealand Journal of Marine and Freshwater Research* **1993**, *27*, 295–307. doi:10.1080/00288330.1993.9516570.

66. Welschmeyer, N.A.; Strom, S.; Goericke, R.; DiTullio, G.; Belvin, M.; Petersen, W. Primary production in the subarctic Pacific Ocean: Project SUPER. *Progress in Oceanography* **1993**, *32*, 101–135. doi:10.1016/0079-6611(93)90010-B.

67. Lindley, S.T.; Bidigare, R.R.; Barber, R.T. Phytoplankton photosynthesis parameters along 140^oW in the equatorial Pacific. *Deep-Sea Research Part II* **1995**, *42*, 441–463. doi:10.1016/0967-0645(95)00029-P.

68. Barber, R.T.; Sanderson, M.P.; Lindley, S.T.; Chai, F.; Newton, J.; Trees, C.C.; Foley, D.G.; Chavez, F.P. Primary productivity and its regulation in the equatorial pacific during and following the 1991-1992 El Nino. *Deep-Sea Research Part II: Topical Studies in Oceanography* **1996**, *43*, 933–969. doi:10.1016/0967-0645(96)00035-5.

69. Vant, W.N.; Safi, K.A. Size-fractionated phytoplankton biomass and photosynthesis in Manukau Harbour, New Zealand. *New Zealand Journal of Marine and Freshwater Research* **1996**, *30*, 115–125. doi:10.1080/00288330.1996.9516701.

70. Gallegos, C.L.; Vant, W.N. An incubation procedure for estimating carbon-to-chlorophyll ratios and growth-irradiance relationships of estuarine phytoplankton. *Marine Ecology Progress Series* **1996**, *138*, 275–291. doi:10.3354/meps138275.

71. Hawes, I.; Gall, M.; Weatherhead, M. Photosynthetic parameters in water masses in the vicinity of the Chatham rise, south pacific ocean, during late summer. *New Zealand Journal of Marine and Freshwater Research* **1997**, *31*, 25–38. doi:10.1080/00288330.1997.9516742.

72. Gibbs, M.M.; Vant, W.N. Seasonal changes in factors controlling phytoplankton growth in Beatrix Bay, New Zealand. *New Zealand Journal of Marine and Freshwater Research* **1997**, *31*, 237–248. doi:10.1080/00288330.1997.9516761.

73. Gall, M.; Hawes, I.; Boyd, P. Predicting rates of primary production in the vicinity of the Subtropical Convergence east of New Zealand. *New Zealand Journal of Marine and Freshwater Research* **1999**, *33*, 443–455. doi:10.1080/00288330.1999.9516890.

74. Macedo, M.F. Annual Variation of Environmental Variables, Phytoplankton Species Composition and Photosynthetic Parameters in a Coastal Lagoon. *Journal of Plankton Research* **2001**, *23*, 719–732. doi:10.1093/plankt/23.7.719.

75. Johnson, Z.; Bidigare, R.R.; Goericke, R.; Marra, J.; Trees, C.; Barber, R.T. Photosynthetic physiology and physicochemical forcing in the Arabian Sea, 1995. *Deep-Sea Research Part I: Oceanographic Research Papers* **2002**, *49*, 415–436. doi:10.1016/S0967-0637(01)00068-1.

76. Aguirre-Hernández, E.; Gaxiola-Castro, G.; Nájera-Martínez, S.; Baumgartner, T.; Kahru, M.; Greg Mitchell, B. Phytoplankton absorption, photosynthetic parameters, and primary production off Baja California: Summer and autumn 1998. *Deep-Sea Research Part II: Topical Studies in Oceanography* **2004**, *51*, 799–816. doi:10.1016/j.dsr2.2004.05.015.

77. Vernet, M. Production vs Irradiance data from RVIB Nathaniel B. Palmer cruise NBP0103 in the Southern Ocean in 2001 (SOGLOBEC project). *Biological and Chemical Oceanography Data Management Office (BCO-DMO)* **2004**, *Dataset v*, 2004–11–18. doi:10.1575/1912/bco-dmo.2375.1.

78. Henríquez, L.A.; Daneri, G.; Muñoz, C.A.; Montero, P.; Veas, R.; Palma, A.T. Primary production and phytoplanktonic biomass in shallow marine environments of central Chile: Effect of coastal geomorphology. *Estuarine, Coastal and Shelf Science* **2007**, *73*, 137–147. doi:10.1016/j.ecss.2006.12.013.

79. Strom, S.L.; Macri, E.L.; Fredrickson, K.A. Light limitation of summer primary production in the coastal Gulf of Alaska: Physiological and environmental causes. *Marine Ecology Progress Series* **2010**, *402*, 45–57. doi:10.3354/meps08456.

80. Huot, Y. MALINA: Photosynthetic parameters. *LEFE CYBER Database* **2011**, *30091*.

81. Menden-Deuer, S. Structure-Dependent phytoplankton photosynthesis and production rates: Implications for the formation, maintenance, and decline of plankton patches. *Marine Ecology Progress Series* **2012**, *468*, 15–30. doi:10.3354/meps09968.

82. Vernet, M.; Wendy, a.K.; Lynn, R.Y.; Alexander, T.L.; Robin, M.R.; Langdon, B.Q.; Christian, H.F. Primary production throughout austral fall, during a time of decreasing daylength in the western Antarctic Peninsula. *Marine Ecology Progress Series* **2012**, *452*, 45–61. doi:10.3354/meps09704.

83. Huot, Y.; Babin, M.; Bruyant, F. Photosynthetic parameters in the Beaufort Sea in relation to the phytoplankton community structure. *Biogeosciences* **2013**, *10*, 3445–3454. doi:10.5194/bg-10-3445-2013.

84. Fuentes-Lema, A.; Sobrino, C.; González, N.; Estrada, M.; Neale, P. Effect of solar UVR on the production of particulate and dissolved organic carbon from phytoplankton assemblages in the Indian Ocean. *Marine Ecology Progress Series* **2015**, *535*, 47–61. doi:10.3354/meps11414.

85. Kovač, Ž.; Platt, T.; Sathyendranath, S.; Morović, M.; Jackson, T. Recovery of photosynthesis parameters from *in situ* profiles of phytoplankton production. *ICES Journal of Marine Science* **2016**, *73*, 275–285. doi:10.1093/icesjms/fsv204.

86. Richardson, K.; Bendtsen, J.; Kragh, T.; Mousing, E.A. Constraining the distribution of photosynthetic parameters in the global ocean. *Frontiers in Marine Science* **2016**, *3*, 269. doi:10.3389/fmars.2016.00269.

87. Strom, S.L.; Fredrickson, K.A.; Bright, K.J. Spring phytoplankton in the eastern coastal Gulf of Alaska: Photosynthesis and production during high and low bloom years. *Deep-Sea Research Part II: Topical Studies in Oceanography* **2016**, *132*, 107–121. doi:10.1016/j.dsr2.2015.05.003.

88. Chakraborty, S.; Lohrenz, S.E.; Gundersen, K. Photophysiological and light absorption properties of phytoplankton communities in the river-dominated margin of the northern Gulf of Mexico. *Journal of Geophysical Research: Oceans* **2017**, *122*, 4922–4938. doi:10.1002/2013JC009262.

89. Endo, H.; Hattori, H.; Mishima, T.; Hashida, G.; Sasaki, H.; Nishioka, J.; Suzuki, K. Phytoplankton community responses to iron and CO2 enrichment in different biogeochemical regions of the Southern Ocean. *Polar Biology* **2017**, *40*, 2143–2159. doi:10.1007/s00300-017-2130-3.

90. Fragoso, G.M.; Poulton, A.J.; Yashayaev, I.M.; Head, E.I.J.; Purdie, D.A. Spring phytoplankton communities of the Labrador Sea(2005–2014): pigment signatures, photophysiologyand elemental ratios. *Biogeosciences* **2017**, *14*, 1235–1259. doi:doi:10.5194/bg-14-1235-2017.

91. Fragoso, G.M.; Poulton, A.J.; Yashayaev, I.M.; Head, E.J.; Purdie, D.A. Spring phytoplankton communities of the Labrador Sea (2005-2014): pigment signatures, photophysiology and elemental ratios. *PANGAEA* **2017**, *871872*. doi:doi.org/10.1594/PANGAEA.871872.

92. Endo, H.; Hattori, H.; Mishima, T.; Hashida, G.; Sasaki, H.; Nishioka, J.; Suzuki, K. Seawater carbonate chemistry and biomarker pigments and phytoplankton community composition in different biogeochemical regions of the Southern Ocean. *PANGAEA* **2018**, *888447*. doi:10.1594/PANGAEA.888447.

93. Briggs, N.; Guemundsson, K.; Cetinić, I.; D'Asaro, E.; Rehm, E.; Lee, C.; Perry, M.J. A multi-method autonomous assessment of primary productivity and export efficiency in the springtime North Atlantic. *Biogeosciences* **2018**, *15*, 4515–4532. doi:10.5194/bg-15-4515-2018.

94. Perry, M.J. Primary productivity measurements from on-deck bottle incubations during R/V Knorr cruise KN193-03 and R/V Bjarni Saemundsson cruises B10-2008 and B4-2008 to the subpolar North Atlantic, Iceland Basin in 2008. *Biological and Chemical Oceanography Data Management Office (BCO-DMO).* **2018**, *Dataset v*, 2018–09–17.

95. Platt, T.; Jassby, A.D. The relationship between photosynthesis and light for natural assemblages of coastal marine phytoplankton. *Journal of Phycology* **1976**, *12*, 421–430.

96. Brewin, R.J.W.; Devred, E.; Sathyendranath, S.; Lavender, S.J.; Hardman-Mountford, N.J. Model of phytoplankton absorption based on three size classes. *Applied Optics* **2011**, *50*, 4535–4549. doi:10.1364/AO.50.004535.

97. Brewin, R.J.W.; Sathyendranath, S.; Jackson, T.; Barlow, R.; Brotas, V.; Airs, R.; Lamont, T. Influence of light in the mixed-layer on the parameters of a three-component model of phytoplankton size class. *Remote Sensing of Environment* **2015**, *168*, 437–450. doi:10.1016/j.rse.2015.07.004.

98. Santer, B.D.; Thorne, P.W.; Haimberger, L.; Taylor, K.E.; Wigley, T.M.L.; Lazante, J.R.; Solomon, S.; Free, M.; Gleckler, P.J.; Jones, P.D.; Karl, T.R.; Klein, S.A.; Mears, C.; Nychka, D.; Schmidt, G.A.; Sherwood, S.C.; Wentz, F.J. Consistency of modelled and observed temperature trends in the tropical troposhpere. *International Journal of Climatology* **2008**, *28*, 1703–1722. doi:10.1002/joc.1756.

99. Kao, H.Y.; Yu, J.Y. Contrasting Eastern-Pacific and Central-Pacific types of ENSO. *Journal of Climate* **2009**, *22*, 615–632. doi:10.1175/2008JCLI2309.1.

100. Lewis, M.; Warnock, R.; Platt, T. Absorption and photosynthesis action spectra for natural phytoplankton populations: implications for prodution in the open ocean. *Limnology and Oceanography* **1985**, *30*, 794–806.

101. Platt, T.; Sathyendranath, S.; Caverhill, C.M.; Lewis, M.R. Ocean primary production and available light: further algorithms for remote sensing. *Deep Sea Research Part A, Oceanographic Research Papers* **1988**, *35*, 855–879. doi:10.1016/0198-0149(88)90064-7.

102. Sathyendranath, S.; Platt, T. Computation of aquatic primary production: Extended formalism to include effect of angular and spectral distribution of light. *Limnology and Oceanography* **1989**, *34*, 188–198.

103. Platt, T.; Sathyendranath, S.; Ravindran, P. Primary prodution by phytoplankton: analytic solutions for daily rates per unit area of water surface. *Proceedings of the Royal Society B: Biological Sciences* **1990**, *241*, 101–111.

104. Sathyendranath, S.; Platt, T.; Brewin, R.J.W.; Jackson, T. Primary Production Distribution. In *Encyclopedia of Ocean Sciences, 3rd Edition*; Cochran, J.K.; Bokuniewicz, J.H.; Yager, L.P., Eds.; Elsevier, 2019; Vol. 1, pp. 635–640. doi:dx.doi.org/10.1016/B978-0-12-409548-9.04304-9.

105. Marañón, E.; Holligan, P.M. Photosynthetic parameters of phytoplankton from 50^oN to 50^oS in the Atlantic Ocean. *Marine Ecology Progress Series* **1999**, *176*, 191–203. doi:10.3354/meps176191.

106. Platt, T.; Sathyendranath, S.; Forget, M.H.; White, G.N.; Caverhill, C.; Bouman, H.; Devred, E.; Son, S. Operational mode estimation of primary production at large geographical scales. *Remote Sensing of Environment* **2008**, *112*, 3437–3448.

107. Xie, Y.; Huang, B.; Lin, L.; Laws, E.A.; Wang, L.; Shang, S.; Zhang, T.; Dai, M. Photosynthetic parameters in the northern South China Sea in relation to phytoplankton community structure. *Journal of Geophysical Research: Oceans* **2015**, *10.1002/20*, 4187–4204. doi:10.1002/2014JC010387.Received.

108. Robinson, A.; Bouman, H.A.; Tilstone, G.H.; Sathyendranath, S. Size class dependent relationships between temperature and phytoplankton photosynthesis-irradiance parameters in the Atlantic Ocean. *Frontiers in Marine Science* **2018**, *4*, 435. doi:10.3389/fmars.2017.00435.

109. Eppley, R.W. Temperature and phytoplankton growth in the sea. *Fishery Bulletin* **1972**, *70*, 1063–1085.

110. Saux Picart, S.; Sathyendranath, S.; Dowell, M.; Moore, T.; Platt, T. Remote sensing of assimilation number for marine phytoplankton. *Remote Sensing of Environment* **2014**, *146*, 87–96. doi:10.1016/j.rse.2013.10.032.

111. Rey, F. Photosynthesis-irradiance relationships in natural phytoplankton populations of the Barents Sea. Proceedings of the Pro Mare Symposium on Polr Marine Ecology, Trondheim, 12-16 May, 1990; Sakshaug, E., Ed. Polar Research, 10, 1991, pp. 105–116.

112. Henson, S.A.; Sarmiento, J.L.; Dunne, J.P.; Bopp, L.; Lima, I.; Doney, S.C.; John, J.; Beaulieu, C. Detection of anthropogenic climate change in satellite records of ocean chlorophyll and productivity. *Biogeosciences* **2010**, *7*, 621–640. doi:10.5194/bg-7-621-2010.

113. Sathyendranath, S.; Platt, T. The spectral irradiance field at the surface and in the interior of the ocean: A model for applications in oceanography and remote sensing. *Journal of Geophysical Research* **1988**, *93*, 9270–9280.

114. Sathyendranath, S.; Cota, G.; Stuart, V.; Maass, H.; Platt, T. Remote sensing of phytoplankton pigments: a comparison of empirical and theoretical approaches. *International Journal of Remote Sensing* **2001**, *22*, 249–273.

115. Morel, A. Optical properties of pure seawater. In *Optical Aspects of Oceanography*; Jerlov, N.G.; Nielsen, E.S., Eds.; Academic: New York, 1974; pp. 1–24.

116. Ulloa, O.; Sathyendranath, S.; Platt, T. Effect of the particle-size distribution on the backscattering ratio in seawater. *Applied Optics* **1994**, *33*, 7070. doi:10.1364/ao.33.007070.

117. Loisel, H.; Morel, A. Light scattering and chlorophyll concentration in case 1 waters: a reexamination. *Limnology and Oceanography* **1998**, *43*, 847–858.

118. Sathyendranath, S.; Platt, P.; Caverhill, C.; Warnock, R.; Lewis, M. Remote sensing of oceanic primary production: computations using a spectral model. *Deep-Sea Research I* **1989**, *36*, 431–453.